Scilight

Sustainable Engineering Novit

https://www.sciltp.com/journals/sen

Article

Design and Fabrication of Metal-Organic Framework UiO-66 Membranes for Advanced Separation

Si Sun [1,2], Yijing Zhang [1,2], Ming Wang [1,2], Rongrong He [3], Zhehua Jia [1], Youhua Zhao [1] and Shenzhen Cong [1,2,*]

[1] School of Chemistry and Chemical Engineering, Yangzhou University, Yangzhou 225009, China
[2] Yangzhou Key Laboratory of Smart Materials and Clean Energy, Yangzhou 225009, China
[3] Jiangsu Scinor Membrane Separation Technology Co., Ltd., Yangzhou 225009, China
* Correspondence: congshenzhen@yzu.edu.cn

How To Cite: Sun, S.; Zhang, Y.; Wang, M.; et al. Design and Fabrication of Metal-Organic Framework UiO-66 Membranes for Advanced Separation. *Sustainable Engineering Novit* **2026**, *2*(1), 3. https://doi.org/10.53941/sen.2026.100003

Received: 14 December 2025
Revised: 19 January 2026
Accepted: 26 January 2026
Published: 27 February 2026

Abstract: UiO-66, a zirconium-based metal-organic framework (MOF) membrane material characterized by exceptional chemical stability and adjustable pore size, has garnered significant interest in the separation domain owing to the synergistic effect of its intrinsic separation properties and the high efficacy of membrane technology. Currently, several methods for producing UiO-66 polycrystalline membranes have been established. Controlling reaction parameters, enhancing the seed layer, and developing composite structures can accurately optimize the membrane's crystallinity, defect density, and interfacial bonding strength, laying a solid structural foundation for its practical uses. UiO-66-based polycrystalline membranes offer superior gas separation performance for mixed gas systems like CO_2/N_2, with higher permeability and selectivity compared to standard membranes. In the realm of nanofiltration, it can accurately retain dyes and tiny organic molecules, indicating a high application potential in wastewater treatment. Pervaporation efficiently dehydrates organic materials, satisfying the purifying needs of the fine chemical sector. In ion separation, ligand functionalization enables the selective removal of various ions, allowing for the enrichment of specific ions. However, UiO-66 polycrystalline membranes have numerous obstacles, including expensive costs for large-scale preparation and poor stability in complex systems. Future study should concentrate on functional modification and innovation in preparation techniques to broaden their industrial uses.

Keywords: polycrystalline UiO-66 membranes; fabrication; gas separation; ion separation; pervaporation

1. Introduction

In the chemical industry, separation refers to the process of purifying a mixture via physical or chemical methods by leveraging differences in the intrinsic properties of its components [1]. Conventional separation technologies, such as distillation, adsorption, and crystallization, are typically energy-intensive [2,3]. Statistical data show that 10–15% of global industrial energy consumption is consumed by separation operations, and this proportion can reach up to 40% in certain sectors (e.g., chemical and petrochemical industries) [1,4]. Consequently, the development of efficient, energy-saving, and environmentally benign separation technologies has become a core focus of scientific research and industrial practice [5]. Compared with conventional separation technologies, membrane separation technology exhibits inherent advantages including lower capital costs, low energy consumption, a compact footprint, and reduced environmental impact, and has been successfully applied in a wide range of industrial fields [6]. The key to achieving excellent separation performance with membrane technology lies in the development of high-performance membrane materials [7–12].

Polymers are currently the most widely used membrane materials in industrial applications, owing to their superior permeability and favorable mechanical properties. However, polymeric membranes suffer from inherent limitations, including a relatively short service life, poor hydrothermal and chemical stability, and low separation selectivity [13–15]. In contrast, zeolitic membranes exhibit distinct advantages such as high selectivity and excellent thermal/chemical stability, laying a solid foundation for their application in separation processes under high-temperature and harsh chemical conditions [16]. Nevertheless, the industrial adoption of zeolitic membranes is constrained by their narrow pore size distribution, high fabrication costs, and inherent difficulty in chemical modification. Metal-organic frameworks (MOFs) represent an emerging class of porous crystalline materials constructed from metal ions or clusters (serving as nodes) and organic ligands linked through coordination interactions [17,18]. Endowed with ultrahigh Brunauer-Emmett-Teller (BET) specific surface area, versatile chemical functionalities, tailorable pore architectures, and superior thermal stability, MOFs exhibit considerable potential as high-performance membrane materials, thereby garnering significant attention in academic and industrial research [19–22]. Beyond separation, MOFs have demonstrated significant potential in gas storage [23], catalysis [24], sensing [25], and drug delivery [26]. However, most MOFs are synthesized in powder form, which renders them unsuitable for direct application in practical separation processes. To realize their industrial utility, MOFs must be processed into continuous, defect-free membranes with robust adhesion to the supporting substrate [27]. The pioneering work on MOF membrane fabrication dates back to 2005, when Fischer et al. fabricated the first MOF thin film by depositing the archetypal MOF-5 onto a functionalized substrate (a self-assembled monolayer (SAM) on a gold surface) [28]. In 2007, Caro et al. reported the in situ crystallization of $[Mn(HCO_3)_2]$ on various porous substrates, elucidating that the surface properties of the substrate modulate crystal growth density [29]. Following this, Bein et al. demonstrated the directed growth of multiple MOFs (e.g., HKUST-1, MIL-53, and MIL-88) on SAM-modified metal substrates [30,31], whereas Gascon et al. developed a denser HKUST-1 membrane on a porous Al_2O_3 substrate via a seed-mediated growth strategy [32]. Notably, none of these early thin films exhibited separation performance [33,34]. A pivotal breakthrough was achieved in 2009, when Lai et al. respective research groups independently reported the fabrication of the first gas separation-compatible MOF membrane by coating MOF-5 onto porous Al_2O_3 substrates [35,36], thereby validating the superior separation potential of MOF-based membranes. Despite this progress, the low chemical stability of many MOFs-particularly under aqueous or acidic conditions-remains a critical barrier to their practical application [37]. Thus, developing MOF materials with enhanced stability is imperative for the fabrication of robust separation membranes.

UiO-66 is a class of MOF materials constructed by the coordination of zirconium clusters with terephthalic acid or its derivatives. It exhibits exceptional hydrothermal and chemical stability, enabling tolerance to strongly polar solvents [38–40]. Based on the Lewis acid/base theory, the robust coordination interactions between Zr^{4+} (hard acids) and terephthalic acid (H_2BDC) ligands (hard bases) confer superior thermodynamic stability upon the UiO-66 framework [41]. Furthermore, the inherent charge imbalance of Zr^{4+} necessitates additional ligand coordination, which facilitates the formation of a densely crosslinked framework and further enhances structural stability [42].

Since its initial report, UiO-66 and its topological analogs have garnered considerable research attention [43,44]. However, the unique growth characteristics and stringent preparation conditions of UiO-66 pose significant challenges to membrane synthesis. Liu et al. [45] successfully fabricated a continuous, defect-free UiO-66 membrane by *in-situ* growth, which was subsequently applied for water softening. This work sparked widespread interest in UiO-66 membranes, and subsequent advancements have been achieved through ligand optimization-enabling precise regulation of pore size and surface functionality [46–48], thereby promoting the development of UiO-66 membranes for diverse separation applications [49–52]. Existing reviews on UiO-66-based membranes are typically characterized by extensive yet superficial coverage, disjointed enumeration of findings, and a predominant focus on fundamental research, which fail to fully exploit the structural advantages and application potential of such membranes. In contrast, the present review, through its core framework featuring precise anchoring to the intrinsic characteristics of UiO-66, establishment of a closed-loop system integrating preparation, mechanism, and application, integration of fundamental and industrial perspectives, systematic clarification of functional modification regulation rules, and construction of a multi-dimensional comparative system, achieves a paradigm shift from mere information compilation to logical integration and value orientation. This review not only provides clear guidance for fundamental research but also offers feasible technical references for industrial-scale applications, thereby filling the gaps of existing reviews in terms of depth, relevance, and application-oriented insights. A systematic overview of the preparation strategies for UiO-66-based membranes/films, discusses their performance in key applications (e.g., gas separation, liquid separation, and ion sieving), and forecasts future advancements in fabrication technologies and industrial applications. The objective is to offer theoretical guidance and technical references for advancing UiO-66-based MOF membranes from fundamental research to practical industrial deployment.

2. The Fabrication of UiO-66-Based Membrane

UiO-66-based membranes are primarily categorized into polycrystalline UiO-66 membranes and UiO-66 nanoparticle-based composite membranes. Polycrystalline UiO-66 membranes can be further divided into supported and unsupported types, depending on the presence of a supporting substrate. Currently, supported polycrystalline UiO-66 membranes account for the majority of reported cases. Porous supports are commonly employed to minimize substrate-induced permeation resistance during separation processes, and the most widely used porous supports include metal oxide substrates (e.g., Al_2O_3, TiO_2), metal substrates (e.g., Cu mesh, stainless steel mesh), alloy substrates (e.g., brass), and polymer substrates (e.g., polysulfone, polyacrylonitrile). The substrate serves as the core supporting framework of UiO-66-based membranes, and its surface chemical properties, pore structural parameters, physicochemical stability, and morphological structure directly determine the nucleation efficiency of UiO-66 crystal nuclei, the compactness and defect density of the membrane layer, and further modulate the separation performance and long-term operational stability of the resultant membranes. Current research on substrate selection mostly relies on empirical trials, lacking systematic correlation analysis of the carrier properties-membrane structure-separation performance paradigm. Specifically, the substrate properties indirectly govern the separation performance by regulating the key structural parameters of the UiO-66 membrane layer, including defect density, pore size, and interfacial adhesion between the membrane and substrate. Based on the geometry of the supporting substrate, polycrystalline UiO-66 membranes are classified as planar, tubular, or hollow fiber membranes [45,49,53–56]. A core challenge in fabricating high-performance polycrystalline UiO-66 membranes lies in regulating the heterogeneous nucleation, crystallization, and intergrowth of UiO-66 on the support surface to minimize non-selective intercrystalline defects. To address this, various synthetic strategies have been explored for preparing defect-free polycrystalline UiO-66 membranes (Table 1), including *in-situ* growth [45,49], secondary growth [57], vapor deposition [58,59], counter-diffusion growth [60] and electrochemical synthesis [61,62].

Table 1. Comparison of the advantages and disadvantages of the preparation methods of UiO-66 membrane.

Preparation Methods	Advantages	Disadvantages
in-situ growth	simplicity of operation, low cost	High defect, uneven membrane thickness
secondary growth	High density, excellent selectivity and controllability	The process is cumbersome and difficult to scale.
vapor deposition	Solvent-free, uniform membrane	The equipment is expensive and the speed is slow
counter-diffusion growth	The membrane thickness is controllable, dense and defect-free	The device is complex and it is difficult to enlarge
electrochemical synthesis	Mild low consumption, strong adhesion, can be functionalized	Low yield, limited support

The *in-situ* growth method entails immersing a porous support (either unmodified or surface-functionalized) in a precursor solution, followed by solvothermal treatment to induce the formation of a continuous UiO-66 membrane on the support surface. Liu et al. [45] successfully fabricated a defect-free UiO-66 membrane on an α-Al_2O_3 substrate via *in-situ* solvothermal synthesis by optimizing key preparation parameters and introducing trace amounts of H_2O into the precursor solution (Figure 1a). Notably, the addition of trace water facilitates the formation of Zr-cluster, a critical prerequisite for constructing high-quality UiO-66 membranes with minimal defects. Subsequently, Liu et al. [45] modified the support substrate to reduce the membrane fabrication cycle: a continuous UiO-66 membrane was grown on the outer surface of an yttria-stabilized zirconia (YSZ) hollow fiber support via *in-situ* growth. They systematically investigated the temporal structural evolution of the UiO-66 membrane, as well as the underlying nucleation and growth mechanisms (Figure 1b,c). Specifically, a thin amorphous gel-like layer formed on the YSZ support surface after 2 h of solvothermal treatment, this phenomenon is attributed to the agglomeration of gel-like particles in the precursor solution, which deposit on the support surface via specific chemical interactions between organic ligands and the support interface, coupled with Brownian motion. UiO-66 nuclei then heterogeneously nucleate at the interface of the gel-like layer and precursor solution, strongly adhering to the support surface. With prolonged solvothermal treatment, the gel-like layer on the support uptakes precursor species from the solution and crystallizes into UiO-66 grains. After 48 h of continuous solvothermal growth, a dense, defect-free UiO-66 membrane layer was achieved (Figure 1c). In a related study, Wei et al. [63] synthesized ultrathin UiO-66-NH_2 membranes in just 1 h via ultrasonication-assisted *in-situ* growth. Sodium formate was added as a modulator during the reaction to promote the generation of a high density of small UiO-66-NH_2 nuclei, which provide abundant heterogeneous nucleation sites and enable the rapid formation of a continuous membrane with uniform thickness.

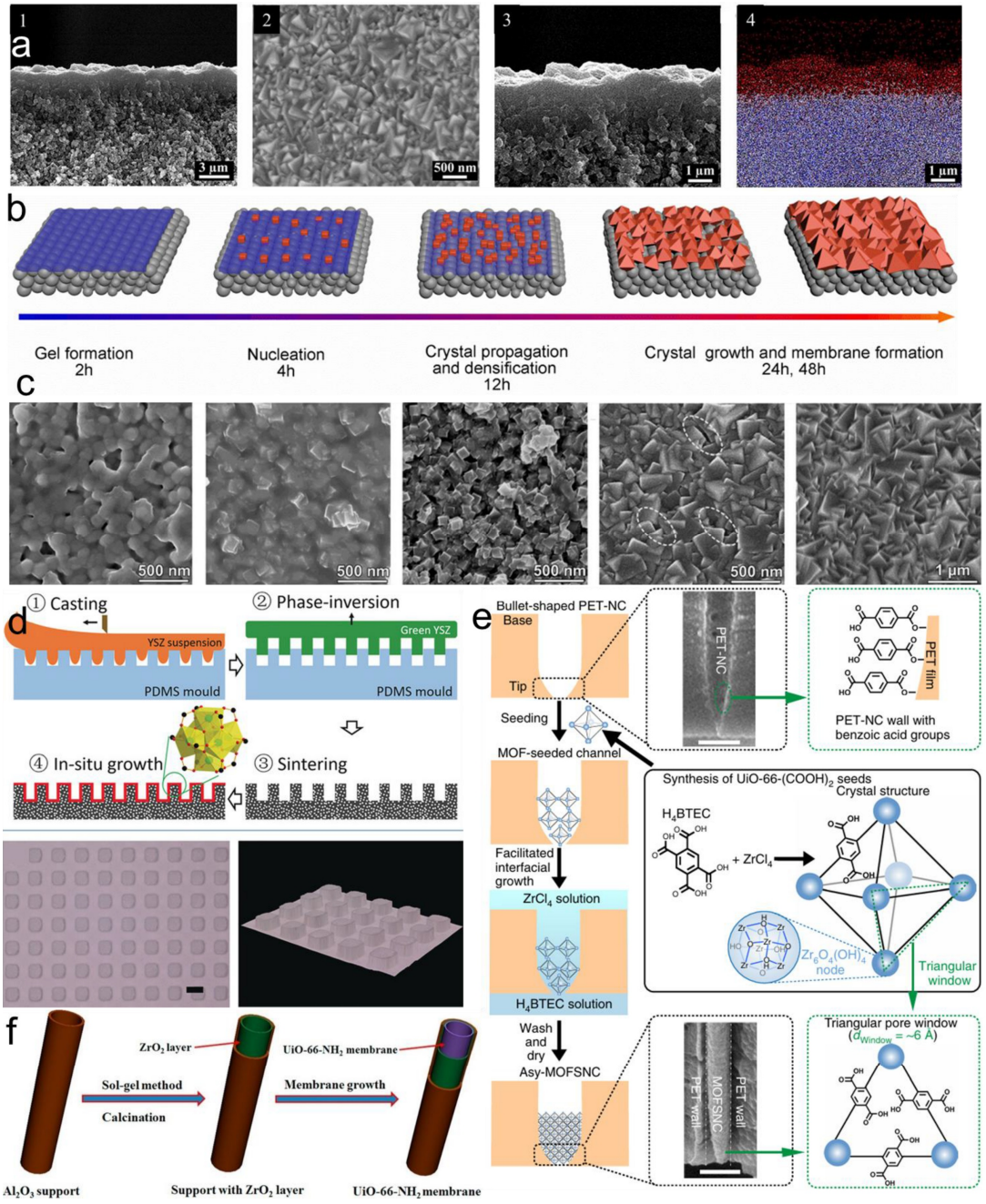

Figure 1. (**a**) Surface (1) and cross-sectional (2) SEM of the UiO-66 membrane fabricated via *in-situ* growth on an α-Al_2O_3 support. Cross-sectional energy-dispersive X-ray spectroscopy (EDXS) mapping (Zr signal, red, Al signal, blue) [45]. Copyright 2016, American Chemical Society. (**b**) Schematic of the *in-situ* growth of the UiO-66 membrane on an yttria-stabilized zirconia (YSZ) substrate. (**c**) Surface SEM of UiO-66 membranes grown on YSZ supports with different growth durations [49]. Copyright 2017, Wiley-VCH (**d**) Schematic of patterned YSZ ceramic substrates and as-prepared UiO-66 membranes [53]. Copyright 2018, Wiley-VCH (**e**) Fabrication process of asymmetric MOF nanocomposite membranes (Asy-MOFSNC) via a facilitated interfacial growth [64]. Copyright 2020, Springer Nature. (**f**) The fabrication process of UiO-66-NH_2 membrane on a ZrO_2 modified α-Al_2O_3 support [65]. Copyright 2018, Elsevier.

To expand the practical applicability of UiO-66 membranes under diverse operating conditions, researchers have explored supports with varied materials and geometries. Huang et al. [53] fabricated UiO-66 membranes with different microstructures via *in-situ* growth (Figure 1d): porous YSZ substrates with tailored microstructures were first prepared via a phase transformation method, then immersed in the precursor solution with the patterned surface facing downward, resulting in continuous, defect-free, ultrathin UiO-66 membranes on the patterned YSZ substrates. Furthermore, Zhang et al. [64] used polyethylene terephthalate (PET) as the support substrate and successfully grown UiO-66 membranes within the nanoscale channels of PET via *in-situ* growth (Figure 1e).

Modifying the support surface to enhance UiO-66 crystal nucleation and growth is a widely adopted strategy for fabricating high-quality UiO-66 membranes. Wu et al. [65] deposited a ZrO_2 transition layer on a porous α-Al_2O_3 support via sol-gel technology, which not only provided critical nucleation sites but also a local zirconium source for UiO-66-NH_2 crystal growth. The well-grown UiO-66-NH_2 membrane was subsequently obtained on the modified α-Al_2O_3 support via *in-situ* solvothermal growth (Figure 1f). Huang et al. [66] functionalized α-Al_2O_3 tubes with 3-aminopropyltriethoxysilane (APTES) and fabricated defect-free NH_2-UiO-66 membranes. Similarly, Ghalei et al. [48] prepared UiO-66 membranes on APTES-modified γ-Al_2O_3 supports via *in-situ* growth; surface functionalization of porous supports with APTES is known to enhance UiO-66 nucleation and intergrowth, facilitating the formation of continuous, defect-free membranes [67]. In another study, Zhang et al. [68] grown acid-base bifunctional UiO-66 membranes on polydopamine-modified polyurethane foam via *in-situ* solvothermal synthesis. By simply adjusting the molar ratio of 2-sulfobenzoic acid to 2-aminobenzoic acid in the UiO-66 framework, they successfully fabricated functionalized UiO-66 membranes with tunable acidity and basicity. Additionally, other substrates have been explored for *in-situ* UiO-66 membrane growth, including ZrO_2 fiber mats [69], fluorine-doped tin oxide (FTO) glass [70], polyacrylonitrile (PAN) fibers [71] and oxidised silicon carbide (ob-SiC) foam [72]. These supports with diverse materials and geometries further broaden the application scope of UiO-66 membranes across various industrial fields.

The secondary growth method for preparing UiO-66 membranes comprises two core steps: seed layer deposition and subsequent UiO-66 membrane growth. This strategy decouples the nucleation and growth stages of crystals, thereby eliminating substrate-imposed constraints on membrane formation. The microstructure of the resulting UiO-66 membranes (e.g., grain density, membrane thickness, crystal orientation) can be precisely tailored by adjusting the size, thickness, and orientation of the seed layer [73,74]. Seed particles used for two-step growth typically meet three key criteria: (1) consistent chemical composition and crystal structure with the target membrane material; (2) narrow particle size distribution to facilitate microstructure control; (3) good dispersibility in a suitable solvent to avoid aggregation during drying.

Wu et al. [75] introduced acetic acid into the growth solution to promote UiO-66 crystal formation and added trace water to assist in the co-assembly of UiO-66 crystals, successfully fabricating a continuous, defect-free UiO-66 membrane on an alumina tube via secondary growth. Mechanistically, zirconium ions can form complexes with various monocarboxylic acids, which mimic the secondary building units (SBUs) of UiO-66. These complexes act as intermediates, facilitating framework construction through ligand exchange at zirconium coordination sites [76–78]. The modifier (acetic acid) reduces the tendency of carboxylic acid ligands to bind directly to SBUs, suppressing undesirable homogeneous nucleation and favoring oriented growth of UiO-66 crystals. Yan et al. [79] deposited a UiO-66 nanoparticle seed layer via spin-coating and employed $Zr_6O_4(OH)_4(OAc)_{12}$ clusters as the zirconium precursor, followed by room-temperature secondary growth to fabricate a continuous, dense, and defect-free UiO-66 membrane (Figure 2a). The use of pre-formed Zr_6 clusters overcomes the high activation energy required for zirconium ion oligomerization. Additionally, adjusting the molar ratio of terephthalic acid ligands to Zr_6 clusters enables precise control of defect site density in the UiO-66 framework, forming a well-interconnected membrane structure. Notably, the UiO-66 membrane fabricated at room temperature exhibits a higher intrinsic defect density, which creates additional gas transport channels and enhances separation performance. Building on this work, Yan et al. [80] constructed an oriented seed layer at the dynamic gas-liquid interface and used pre-synthesized $Zr_6O_4(OH)_4(OAc)_{12}$ clusters to grow UiO-66 membranes at room temperature (Figure 2b). Intercrystalline defects were effectively eliminated through rational structural design, engineered defect management, and controlled crystal growth orientation. In another study, Yan et al. [81] introduced a ZrO_2 buffer layer on a porous α-Al_2O_3 support, followed by spin-coating an oriented UiO-66 seed layer, and fabricated UiO-66 membranes via secondary growth using $Zr(n\text{-}OPr)_4$ as the zirconium precursor (Figure 2c).

Friebe et al. [82] prepared (002)-oriented UiO-66 membranes by UiO-66 crystals initially grew on a randomly oriented seed layer and preferentially propagated along the fastest growth direction (i.e., the (002) plane) over time, forming an oriented membrane. SEM images of the membrane surface showed octahedral crystal vertices, consistent with the van der Waals epitaxial growth mechanism [83]. Sun et al. [84] exploited the dynamic gas-liquid interface to assemble and deposit an oriented seed layer, forming a densely packed monolayer of uniform octahedral NH_2-UiO-66 nanocrystals with (111) orientation. Using ZrS_2 as the zirconium precursor, they fabricated a (111)-oriented NH_2-UiO-66 membrane via two-step hydrothermal epitaxial growth (Figure 2d). Yan et al. [85] adopted a similar strategy, using a dynamic gas-liquid interface for oriented seed layer deposition and ZrS_2 as the zirconium source to prepare (111)-oriented UiO-66 membranes via two-step growth. Rong et al. [86] used layered ZrS_2 (a typical two-dimensional transition metal dichalcogenide, TMDC) as the metal source to fabricate a continuous, defect-free UiO-66 membrane on a porous α-Al_2O_3 substrate via two-step hydrothermal growth. Compared to other zirconium precursors (e.g., $ZrCl_4$), ZrS_2 exhibits superior water and hydrothermal stability,

which suppresses unwanted side reactions, regulates UiO-66 nucleation and growth, and reduces intercrystalline defects. However, the low reactivity of ZrS_2 leads to residual defects in the membrane after two-step growth, necessitating a three-step hydrothermal process to further minimize intercrystalline flaws.

Li et al. [87] developed a hybrid strategy: an *in-situ* grown nanocrystalline seed layer was subjected to further secondary growth to produce a high-quality, stable UiO-66 membrane. To address the challenges of membrane fabrication on coarse mullite substrates, a TiO_2 nanolayer was introduced as an interlayer to support the formation of the UiO-66 nanocrystalline seed layer. A UiO-66 membrane was successfully fabricated on this seed layer via secondary growth (Figure 2e). Subsequently, Wang et al. [88] proposed a strategy combining molecular-level defect engineering and interlayer thinning to design a stable ultrathin UiO-66 membrane with missing linkers (ML-UiO-66). A nanoporous γ-Al_2O_3 interlayer was deposited on a pristine substrate, providing abundant heterogeneous nucleation sites and reducing surface roughness (Figure 2f). The linker defects in the UiO-66 framework created defect-assisted transport pathways, resulting in a membrane with enhanced separation performance.

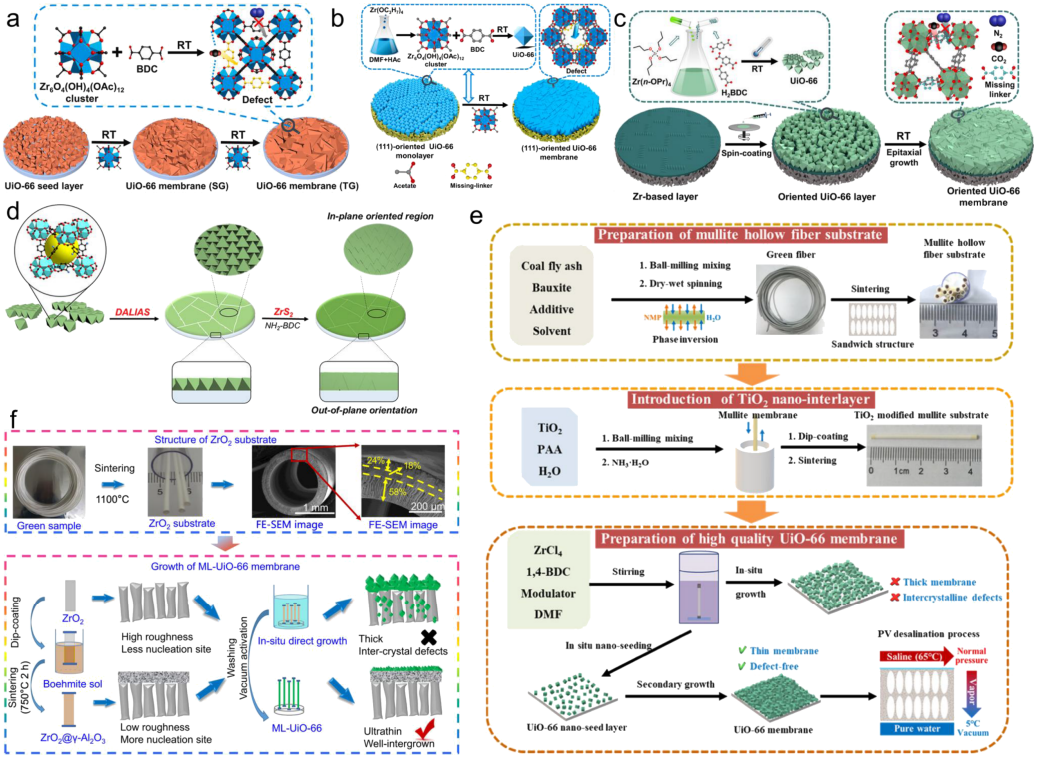

Figure 2. (**a**) Schematic of UiO-66 membrane fabrication by using $Zr_6O_4(OH)_4(OAc)_{12}$ clusters [79]. Copyright 2022, Elsevier. (**b**) Schematic of a highly (111)-oriented, defect-engineered UiO-66 membrane [80]. Copyright 2022, Elsevier. (**c**) Schematic of the preparation process for defect-engineered (111)-oriented UiO-66 membranes [81]. Copyright 2023, American Chemical Society. (**d**) Schematic illustration of the preparation process for an NH_2-UiO-66 membrane with (111) out-of-plane orientation [84]. Copyright 2020, American Chemical Society. (**e**) The preparation process for a UiO-66 membrane [87]. Copyright 2021, American Chemical Society. (**f**) Schematic illustration of the preparation process for a missing-linker UiO-66 (ML-UiO-66) membrane with γ-Al_2O_3 as the intermediate layer [88]. Copyright 2022, Springer Nature.

By fabricating a crystalline interlayer via *in-situ* growth followed by secondary growth of the UiO-66 membrane, interfacial defects can be effectively mitigated, and the interfacial adhesion between the UiO-66 separation layer and the substrate can be significantly enhanced [89,90]. Zhao et al. [91] developed an *in-situ* solvothermal synthesis strategy to fabricate a polycrystalline UiO-66-NH_2 membrane on a low-cost, flexible carbon fiber fabric. Hydrolysis of the carbon substrate generates abundant carboxyl groups, which serve as heterogeneous nucleation sites for UiO-66-NH_2 growth and reinforce the interfacial adhesion between UiO-66-NH_2 and the substrate (Figure 3a). The resulting UiO-66(Zr)-NH_2 membrane has a thickness of less than 1 μm, exhibits excellent mechanical flexibility, and can withstand a bending angle of up to 10°. Xu et al. [92] proposed a method for the *in-situ* fabrication of crown ether@UiO-66 membranes under mild conditions: anodic aluminum oxide (AAO) substrates were first pre-treated with terephthalic acid to form a crystalline interlayer, followed by a secondary growth step where dibenzo-18-crown-6 (DB18C6) or dibenzo-15-crown-5 molecules were precisely incorporated into the pores of the UiO-66 framework (Figure 3b). Using a similar strategy, Xu et al. [93] introduced

1,5-naphthalene disulfonic acid tetrahydrate (NTDS) molecules (bearing sulfonic acid groups) into the UiO-66 framework, fabricating a UiO-66@NTDS composite membrane by synergistically combining the ion affinity of NTDS with the tailored pore structure of UiO-66 (Figure 3c). Sun et al. [94] reported a heterogeneous nucleation-assisted growth approach for fabricating thin, defect-free UiO-66 membranes: the addition of trace water to the precursor solution induced the heterogeneous nucleation of UiO-66 crystals on the substrate surface (Figure 3d). Furthermore, a smooth polydimethylsiloxane (PDMS) interlayer not only ensured robust interfacial adhesion between the crystals and the substrate but also provided a hydrophobic microenvironment. This work presents a novel strategy for constructing high-quality MOF membranes, expanding their applicability in practical gas separation processes. In addition, the secondary growth method can be used to combine UiO-66 with other MOFs to fabricate polycrystalline composite membranes, which feature a hierarchical porous structure with multi-level molecular sieving capabilities, thereby synergistically enhancing separation performance [95–97].

Post-synthetic modification (PSM) is another effective strategy to eliminate intercrystalline defects and optimize the separation performance of UiO-66 membranes [98]. For instance, Huang et al. [99] added salicylic acid during the synthesis of UiO-66-NH_2, which significantly improved its gas separation efficiency. Liu et al. [100] modified UiO-66-NH_2 membranes with various small-molecule acids, greatly expanding their applicability in membrane-based permeation separation. Asadnia et al. [101] constructed an ion channel network with abundant carboxyl functional groups via PSM of zirconium-based MOFs, achieving tunable ion permeability and selectivity. The ion selectivity of this novel MOF membrane is regulated by the surrounding ionic environment and can be switched via selective ion activation, leading to enhanced separation performance. Wang et al. [102] described a method for fabricating a ZrO_2-supported UiO-66-NH_2 membrane, which was subsequently modified with salicylaldehyde. The pore size of the resulting post-modified UiO-66-NH_2 (P-UiO-66-NH_2) membrane was tailored to 0.37 nm, significantly boosting its molecular separation performance.

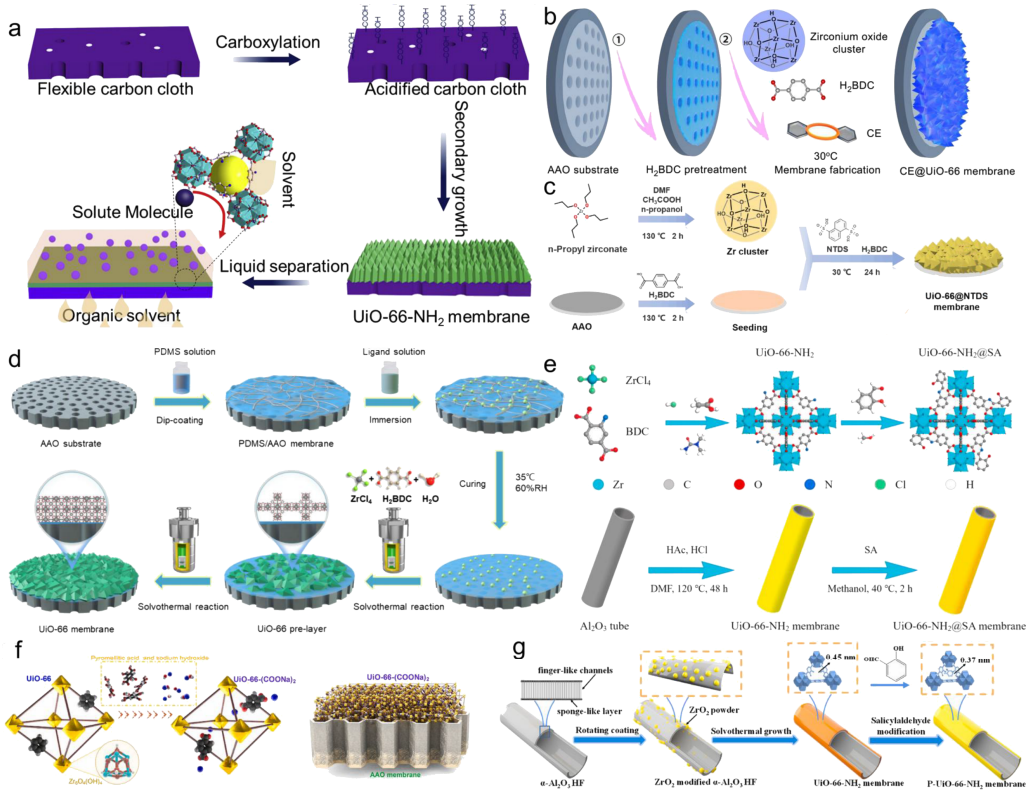

Figure 3. (**a**) Preparation process of flexible carbon cloth supported polycrystalline UiO-66-NH_2 membrane [91]. Copyright 2020, Elsevier. (**b**) Schematic diagram of CE@UiO-66 membrane preparation process [92]. Copyright 2024, American Association for the Advancement of Science. (**c**) Schematic diagram of UiO-66@NTDS membrane preparation process [93]. Copyright 2024, Elsevier. (**d**) Schematic diagram of UiO-66 membrane preparation process using heterogeneous nucleation-assisted growth strategy [103]. Copyright 2024, Elsevier. (**e**) Schematic diagram of UiO-66-NH_2@SA membrane synthesis process by post-synthesis modification [99]. Copyright 2021, Elsevier. (**f**) Schematic for the preparation of UiO-66-$(COONa)_2$ membranes [101]. Copyright 2023, Elsevier. (**g**) Schematic of the preparation process for hollow fiber supported UiO-66-NH_2 membranes [102]. Copyright 2023, Elsevier.

Gas-phase deposition is a versatile thin-film deposition technique that involves depositing a thin solid film, formed via chemical reactions, onto a substrate surface [104,105]. The deposited film is typically composed of atoms, molecules, or their composites. In this process, two or more gas-phase precursors are separately introduced into a reaction chamber, where they undergo heterogeneous reactions at the substrate surface, saturate the interface, and subsequently deposit as a thin layer that crystallizes to form a membrane with tailored morphology and crystal structure. Unlike solvent-mediated nucleation/growth-based fabrication methods (e.g., solvothermal synthesis), gas-phase deposition offers inherent advantages including scalability, solvent-free operation, seedlessness, and precise thickness control, making it compatible with non-planar (irregular) substrates.

Notably, several studies have demonstrated the feasibility of gas-phase deposition for fabricating UiO-66-based membranes. Lausund et al. [106,107] first coated a substrate with an amorphous organic-inorganic hybrid powder, synthesized via the reaction between zirconium chloride and terephthalic acid, followed by acetic acid vapor treatment to induce crystallization, thereby fabricating UiO-66 polycrystalline membranes via gas-phase deposition (Figure 4a). In another work, Virmani et al. [108] utilized gas-phase deposition to synthesize highly oriented UiO-66-NH_2 membranes on self-assembled monolayer (SAM)-modified gold surfaces. The resulting UiO-66-NH_2 membranes exhibited excellent crystallinity; by systematically varying process parameters (e.g., acetic acid dosage, precursor concentration, temperature, and reaction time), the authors elucidated the correlation between crystallization kinetics and the formation of oriented MOF membranes (Figure 4b).

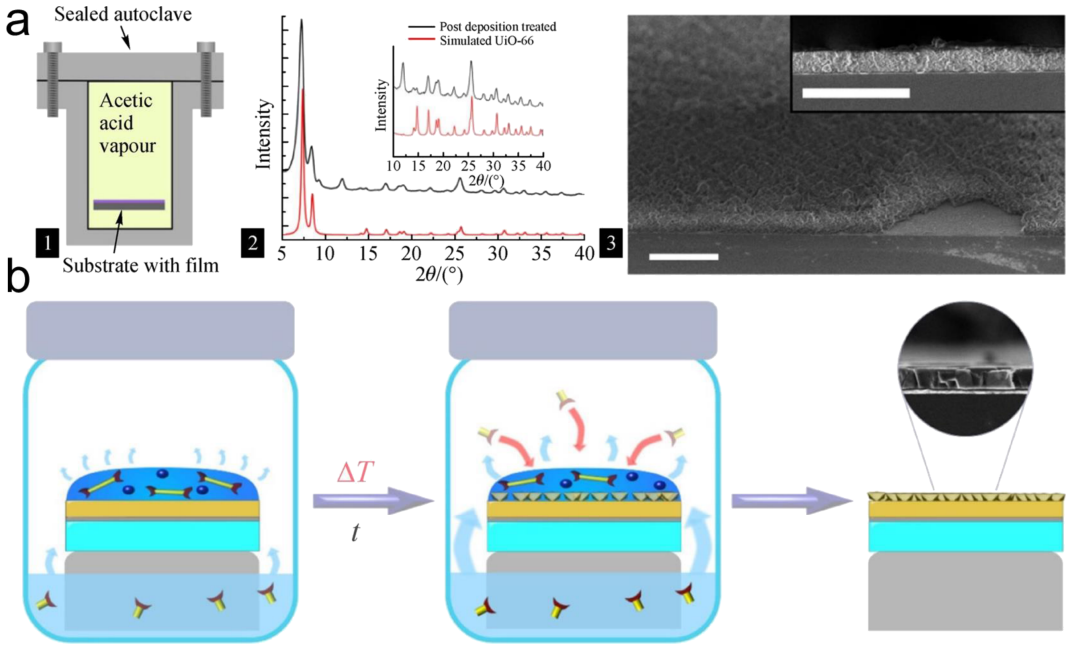

Figure 4. (**a**) (1) The device for acetic acid vapor post-treatment of thin membranes; (2) XRD patterns of the resultant UiO-66 membrane; (3) cross-sectional SEM of UiO-66 membranes [106]. Copyright 2016, Springer Nature. (**b**) Steam-assisted fabrication of (111)-oriented UiO-66-NH_2 membranes [108]. Copyright 2018, American Chemical Society.

The counter-diffusion interfacial growth method for UiO-66 membrane fabrication utilizes a porous support as a "barrier" to separate metal ion and organic ligand solutions on opposite sides. Following counter-directional diffusion, metal ions and organic ligands meet at the support interface, where they undergo collision, heterogeneous nucleation, crystallization, and intergrowth to form a continuous, dense UiO-66 membrane. This technique enables precise regulation of crystal nucleation/growth kinetics and membrane growth rate by tuning the diffusion rate of precursors across the support. Furthermore, homogeneous nucleation (competitive bulk-phase nucleation) can be suppressed by accelerating precursor diffusion via conventional heating or microwave irradiation [109,110]. A key advantage of the counter-diffusion interfacial growth method is its self-terminating reaction behavior: once a dense membrane layer is formed, precursor diffusion is blocked, immediately halting further nucleation and growth.

Metal-organic frameworks (MOFs) offer diverse structural functionalities and tunable pore topologies, making them ideal for precise molecular separation. However, fabricating defect-free MOF membranes with high water stability and interconnected porosity remains a critical challenge, primarily due to the difficulty in controlling nucleation and growth rates during synthesis. To address this, Sun et al. [74] deposited etched UiO-66 nanosheets as a seed layer on the support via vacuum filtration, then employed the counter-diffusion interfacial

growth method to heal defects between nanosheets, preserving nanosheet thickness while forming a continuous, defect-free, and highly oriented UiO-66 membrane (Figure 5a). Subsequently, Sun et al. [111] combined hollow-structured UiO-66 seeds with epitaxial growth under single-mode microwave heating to fabricate a hierarchical defect-rich UiO-66 membrane (Figure 5b). This membrane integrated three key structural features: an ultra-thin directionally selective top layer, a hollow-structured bottom layer, and a high density of missing linkers in the framework.

A major bottleneck limiting the performance of MOF membranes for molecular separation is the elimination of atomic-scale lattice defects. Defects enlarge effective pore sizes, compromising separation efficiency, while structural instability restricts their practical application in liquid-phase separation. To overcome this, Jin et al. [112] proposed a highly efficient theoretical coordination strategy: during the interfacial diffusion process for UiO-66 membrane fabrication, they enhanced the chemical interactions between metal clusters and ligands to eliminate lattice defects. This high-probability coordination approach formed a robust framework barrier by enabling complete ligand coordination to metal clusters, overcoming steric hindrance. Building on this, Jin et al. [113] developed a confined coordination-induced co-growth strategy to fabricate defect-free zirconium-based MOF membranes for precise molecular separation (Figure 5c). By controlling precursor counter-diffusion, modulating confined coordination space, and adjusting the reaction environment (e.g., solvents), the coordination reaction rate was slowed, allowing MOF crystals to co-grow into a continuous membrane structure. The resulting zirconium-based MOF membranes featured sub-nanometer pore sizes and exhibited excellent performance in gas separation and seawater desalination. Additionally, Jin et al. [114] successfully fabricated dense, polycrystalline UiO-66 membranes on polymer substrates via interfacial diffusion growth under mild conditions (low temperature and short synthesis time), which demonstrated rapid and selective water transport with outstanding separation performance (Figure 5d).

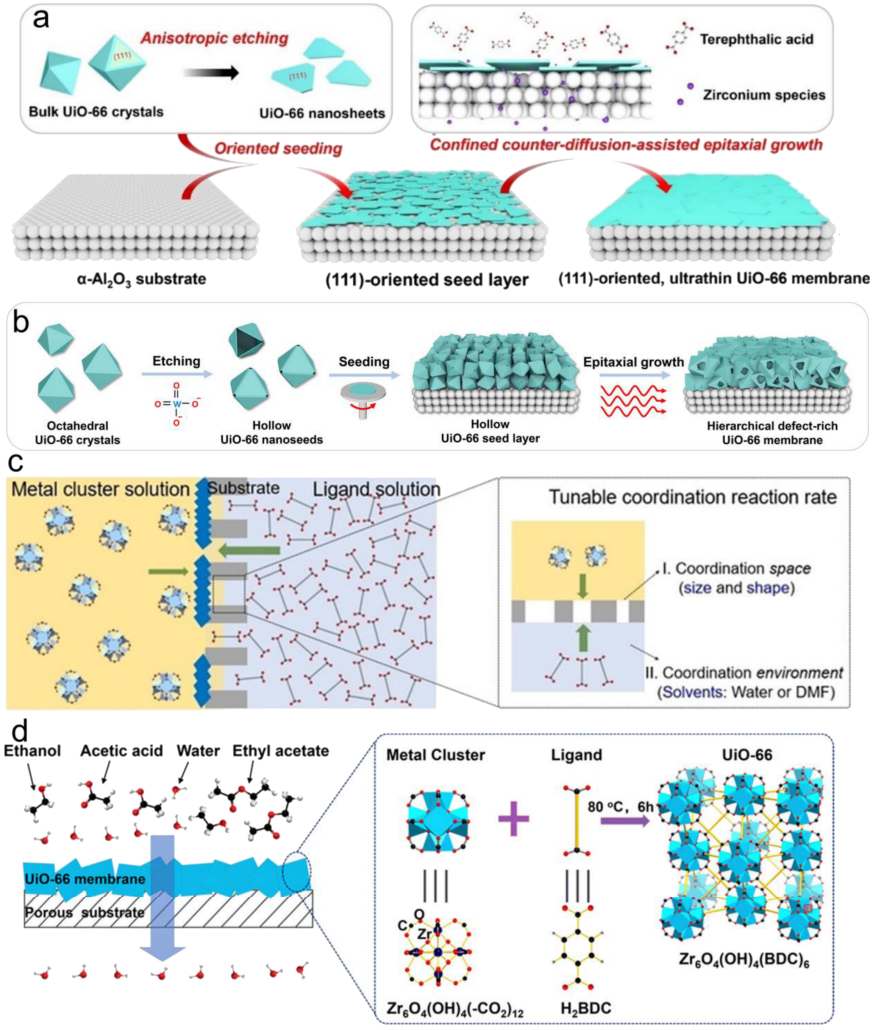

Figure 5. (**a**) Schematic of epitaxial growth of well-intergrown ultrathin UiO-66 membranes [74]. Copyright 2023, Wiley-VCH. (**b**) Schematic of the preparation of hierarchical defect-rich UiO-66 membranes [111]. Copyright 2024, Elsevier. (**c**) Fabrication of a defect-free UiO-66 membrane with intrinsic lattice pores on the substrate [113]. Copyright 2024, Wiley-VCH. (**d**) Illustration of polycrystalline UiO-66 membranes for water/organic solvent separation [114]. Copyright 2023, The Royal Society of Chemistry.

Electrochemical deposition is a thin-film fabrication technique that utilizes an external electric field to drive the migration of cations and anions in a growth solution, facilitating electron transfer and membrane deposition on an electrode surface [115]. It is regarded as a promising strategy for *in-situ* deposition on conductive substrates and is classified into anodic and cathodic deposition based on distinct reaction mechanisms. In anodic deposition, dissolution of the metal anode releases a critical concentration of metal ions, which react with ligands to form a MOF layer on the metal surface [116]. In cathodic deposition, contact between a solution containing metal ions and ligands and the cathode surface induces a local pH increase, promoting MOF nucleation and growth on the cathode [117,118].

Notably, several studies have applied electrochemical deposition for UiO-66 membrane fabrication. Xie et al. [118] (Figure 6). reported a rapid, facile, and controllable method for direct fabrication of UiO-66 thin films via cathodic electrodeposition (Figure 6): lithium nitrate was used to accelerate the deprotonation of terephthalic acid ligands, enabling the preparation of a continuous polycrystalline UiO-66 membrane in just 1 h. Stassen et al. [119] fabricated UiO-66 thin membranes on zirconium substrates via electrochemical deposition: anodic deposition yielded excellent adhesion of the UiO-66 seed layer to the zirconium substrate (attributed to the formation of an oxide interlayer), while cathodic deposition offered broader substrate compatibility. Hod et al. [120] prepared UiO-66 thin coatings on conductive glass via electrochemical deposition: a direct current electric field was applied to a suspension of charged particles in a non-polar solvent, facilitating particle migration and deposition onto the conductive substrate. During UiO-66 synthesis, metal node defects in the framework imparted a net negative charge to the membrane surface, which drove particle attraction to the positively charged electrode and subsequent membrane formation. Zhou et al. [61] fabricated continuous, defect-free UiO-66 coatings on porous anodic aluminum oxide (AAO) via electrochemical deposition, successfully preparing face-centered cubic UiO-66 membranes based on 12-coordinated Zr_6 clusters using an electrochemical self-assembly strategy, demonstrating the compatibility of electrochemical synthesis with supramolecular chemistry.

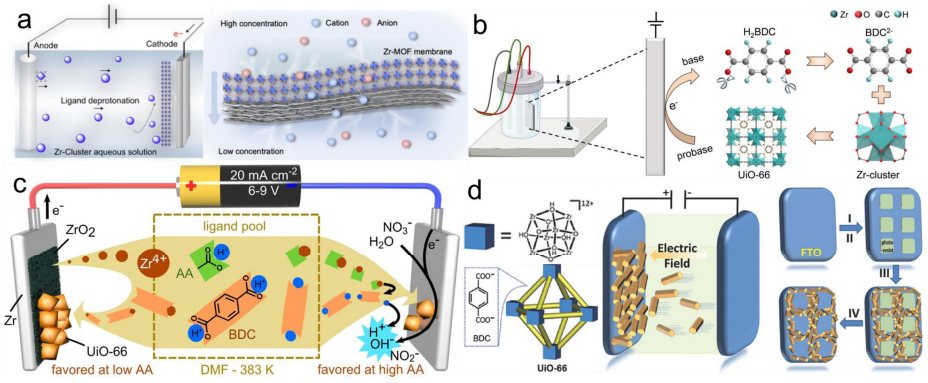

Figure 6. (**a**) Schematic of the electrochemical cell used for the fabrication of zirconium-based metal-organic framework (Zr-MOF) membranes [121]. Copyright 2025, Elsevier. (**b**) Schematic of nitrate-assisted cathodic electrodeposition of UiO-66 membranes [118]. Copyright 2023, Elsevier. (**c**) Schematic of the anodic and cathodic electrodeposition mechanisms proposed [119]. Copyright 2015, American Chemical Society. (**d**) Schematic illustration of the growth principle of MOF electrophoretic deposition (EPD) films, depicting the attraction of charged MOF particles to an oppositely charged electrode under an applied electric field [120]. Copyright 2014, Wiley-VCH.

3. UiO-66 Membranes for Advanced Separation

UiO-66-based membranes feature a versatile and tunable structure, with readily modifiable functional groups and pore diameters. The phenyl rings and substituents of the ligands, as well as the -OH groups on the secondary building units (SBUs), provide abundant adsorption sites, rendering these membranes well-suited for various separation processes. Below is a systematic summary of the applications of UiO-66-based membranes in gas separation, nanofiltration, pervaporation, and ion separation, with a focus on gas separation performance [61].

3.1. Gas Separation

Gas separation membranes achieve gas fractionation based on differences in gas permeation rates through the membrane matrix. Gas permeation occurs when gas molecules contact the membrane surface and diffuse across the membrane under a pressure or partial pressure gradient. The separation mechanism relies on variations in adsorption capacity and diffusion rate of different gas components within the membrane: gases with higher permeability are enriched on the permeate side, while less permeable gases remain on the feed side [122].

Compared to conventional gas separation technologies, membrane-based separation offers inherent advantages, including low energy consumption, facile operation, simple equipment configuration, and high operational stability. While the intrinsic pore size of UiO-66 (~6.0 Å) exceeds the kinetic diameters of most gas molecules (e.g., H_2: 2.89 Å, N_2: 3.64 Å, CO_2: 3.3 Å), thus constraining the efficacy of diffusion-governed separation, its abundant surface adsorption sites enable selective gas fractionation via adsorption-dominated mechanisms. Liu et al. [45] developed *in-situ* grown UiO-66 membranes for gas separation, which delivered an optimal H_2/N_2 selectivity of 22.4 and an H_2 permeance of ~2150 GPU (Gas Permeation Unit, 1 GPU = 3.35×10^{-10} mol·m^{-2}·s^{-1}·Pa^{-1}). Notably, the membrane achieved a CO_2 permeance of 2880 GPU with an ideal CO_2/N_2 selectivity of 29.7, a performance attributed to the preferential adsorption of CO_2 by the hydroxyl (-OH) groups within the UiO-66 framework. Wu et al. [123] further corroborated a consistent gas permeation sequence for UiO-66 membranes, providing additional validation for its adsorption-driven separation mechanism. Defect engineering has emerged as a pivotal strategy to augment the gas separation performance of UiO-66 membranes. Yan et al. [79] constructed a well-interconnected UiO-66 membrane using zirconium clusters under ambient temperature conditions (Figure 7): the membrane's elevated intrinsic defect density facilitated CO_2 mass transport, while interactions between defect sites enhanced CO_2/N_2 selectivity, yielding a separation factor of 37.8 via a three-step room-temperature synthesis protocol. Expanding on this approach, Yan et al. [80] engineered a highly (111)-oriented UiO-66 membrane with precisely tuned defect density for CO_2/N_2 separation. By employing $Zr_6O_4(OH)_4(OAc)_{12}$ clusters as the zirconium precursor for epitaxial growth, the team achieved an optimal CO_2/N_2 selectivity of up to 46.2 (Figure 7d, Table 2). In a follow-up investigation, Yan et al. [81] introduced microscale structural defects into the UiO-66 lattice by adopting ZrS_2 as the metal source during solvothermal synthesis, which augmented ligand vacancies in the framework and promoted preferential CO_2 adsorption; the resultant membrane demonstrated a CO_2/N_2 selectivity of up to 35.6 (Figure 7e, Table 2).

Oriented growth control represents another effective avenue to mitigate mesoscale grain boundary imperfections and enhance MOF membrane performance, though regulating microscale structural defects to boost separation efficiency remains a persistent challenge. Yan et al. [85] pioneered a three-step directed growth methodology to fabricate (111)-oriented UiO-66 membranes: the use of ZrS_2 as the metal source during solvothermal synthesis increased the population of undercoordinated metal sites in the framework, thereby enhancing CO_2 adsorption capacity. In comparison to the two-step growth process, the three-step strategy yielded a UiO-66 membrane with substantially improved CO_2/N_2 selectivity and CO_2 permeance (Figure 7f).

Sun et al. [84] integrated directed deposition with solvothermal co-crystallization to develop an ordered NH_2-UiO-66 membrane featuring (111) out-of-plane orientation and partial in-plane alignment. A dynamic gas-liquid interface-assisted self-assembly technique was utilized to construct a densely packed monolayer of uniform octahedral NH_2-UiO-66 nanocrystals, achieving the targeted crystalline orientation. Furthermore, the adoption of ZrS_2 as the zirconium precursor during solvothermal co-crystallization proved critical for sealing intergrain voids and retaining the crystalline alignment inherited from the nanocrystal layer. Microwave heating resulted in inferior intercrystalline co-crystallization compared to solvothermal heating, which was attributed to the lower dielectric loss of the reaction medium, an effect that compromised uniform energy propagation for crystal intergrowth. Gas separation performance revealed that, under identical operating conditions, the as-prepared NH_2-UiO-66 membrane exhibited a 5.5-fold higher H_2/CO_2 selectivity and a 14.5-fold higher H_2 permeance than randomly oriented or exclusively out-of-plane oriented counterparts (Figure 7g).

Table 2. Summary of the gas separation performance and the preparation methods of UiO-66 membrane.

Membrane	Preparation Methods	Permeance (GPU)	Seletivity	Feed Condition	Ref.
UiO-66	*In-situ* growth	2151 (CO_2)	22.4 (CO_2/N_2)	1 bar, 298 K	[45]
UiO-66/PDA	Secondary growth	1036 (CO_2)	51.3 (CO_2/N_2)	1 bar, 298 K	[123]
UiO-66-CH_3	Secondary growth	5672 (CO_2)	2.2 (CO_2/N_2)	1 bar, 298 K	[55]
UiO-66 (TG)	Tertiary growth	1216 (CO_2)	27.6 (CO_2/N_2)	1 bar, 298 K	[86]
UiO-66	Secondary growth	63 (CO_2)	33.5 (CO_2/N_2)	1 bar, 298 K	104
UiO-66	Counter-diffusion growth	2070 (CO_2) 2070 (H_2)	35.4 (CO_2/N_2) 41.3 (H_2/CO_2)	1 bar, 298 K	[74]
UiO-66	Counter-diffusion growth	~1200 (H_2)	~67 (H_2/CO_2)	1 bar, 298 K	[113]
UiO-66	Tertiary growth	1126 (CO_2)	35.6 (CO_2/N_2)	1 bar, 298 K	[85]
COF@UiO-66	Secondary growth	903 (H_2)	32.9 (H_2/CO_2)	1 bar, 298 K	[124]
UiO-66	Secondary growth	530 (CO_2)	24.3 (CO_2/N_2)	1 bar, 298 K	[103]
UiO-66	*In-situ* growth	336 (CO_2)	15.4 (CO_2/N_2)	1 bar, 298 K	[125]
UiO-66	Secondary growth	1129 (CO_2)	36.5 (CO_2/N_2)	1 bar, 298 K	[81]
UiO-66	Counter-diffusion growth	2129 (CO_2)	35.4 (CO_2/N_2)	1 bar, 298 K	[111]
UiO-66	Secondary growth	1356 (H_2)	5.1 (H_2/CO_2)	1 bar, 298 K	[82]
UiO-66-NH_2@SA	Secondary growth	347 (H_2)	7.3 (H_2/CO_2)	1 bar, 298 K	[99]
UiO-66	Secondary growth	126 (CO_2)	37.8 (CO_2/N_2)	1 bar, 298 K	[79]
P-UiO-66-NH_2	Secondary growth	817 (H_2)	21.7 (H_2/CH_4)	1 bar, 298 K	[102]
UiO-66-NH_2	Secondary growth	96 (CO_2)	40 (CO_2/ CH_4)	1 bar, 298 K	[63]

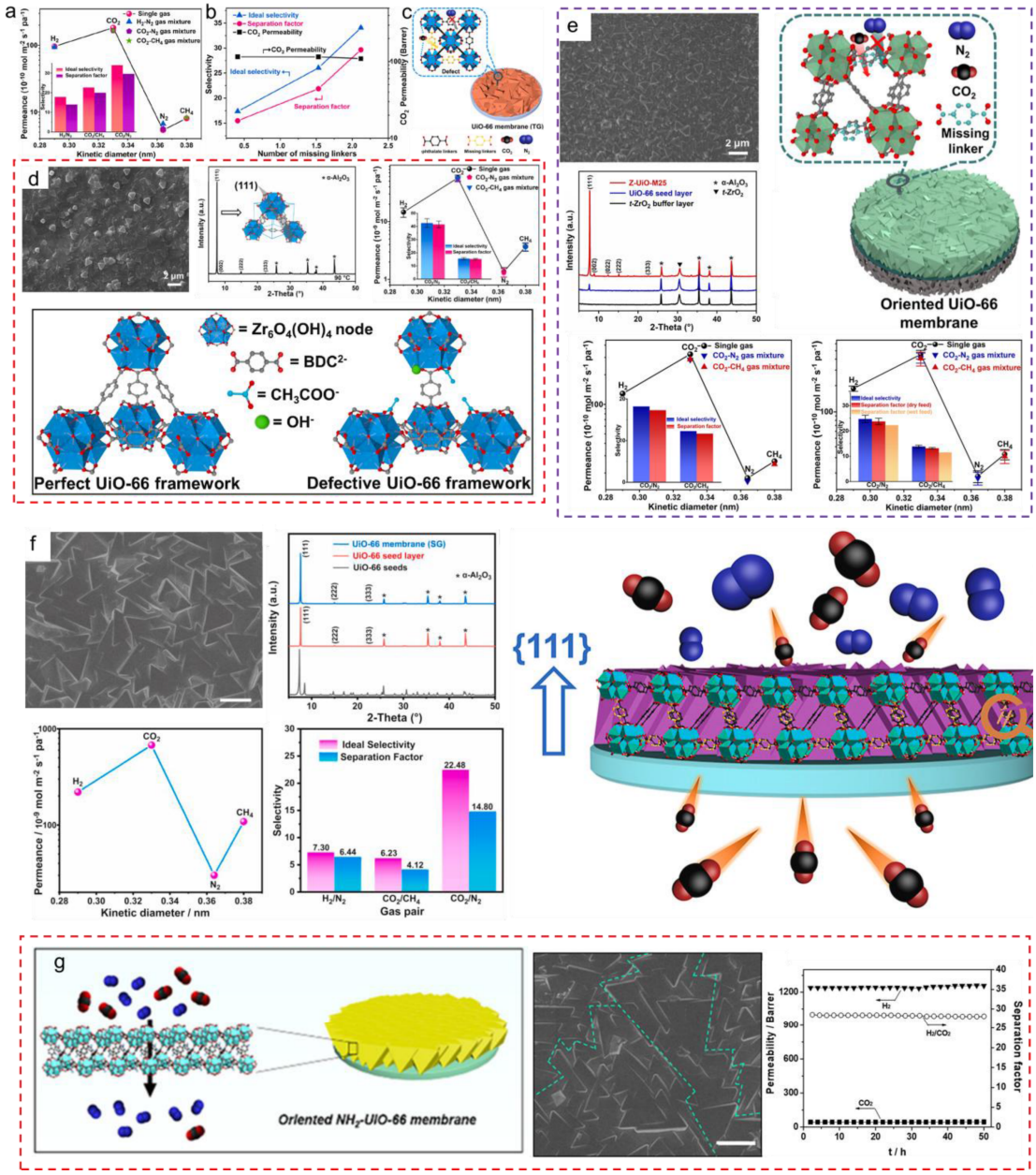

Figure 7. (**a**) Gas permeation results of the UiO-SG$_{25/1.4}$ membrane. (**b**) Correlation between the number of missing linkers per $Zr_6O_4(OH)_4$ node and CO_2 separation performance of UiO-66 membranes. (**c**) Schematic of CO_2/N_2 separation via coordination defects in UiO-66 membranes [79]. Copyright 2022, Elsevier. (**d**) SEM, XRD and single-gas and mixed-gas separation performance of (111)-oriented UiO-66 membranes [80]. Copyright 2022, Elsevier. (**e**) SEM and corresponding XRD patterns of oriented UiO-66 membranes; separation performance of UiO-66 membranes [81]. Copyright 2023, American Chemical Society. (**f**) SEM and corresponding XRD patterns of oriented UiO-66 membranes [85]. Copyright 2021, Elsevier. (**g**) Magnified top and cross-sectional views of the as-prepared NH_2-UiO-66 seed layer on an α-Al_2O_3 substrate [84]. Copyright 2020, American Chemical Society.

3.2. Nanofiltration

Nanofiltration (NF) is a pressure-driven membrane separation technology, which has emerged as a research hotspot in membrane science. NF achieves efficient separation via size sieving and electrostatic repulsion, with pressure as the driving force. Currently, the primary applications of UiO-66-based membranes in NF include hard water softening, desalination, and dye separation from organic solvents [45,124–127].

Liu et al. [45] fabricated an *in-situ* grown UiO-66 membrane for hard water softening, leveraging size-selective filtration to effectively remove multivalent cations: the rejection rates for Ca^{2+} (hydrated diameter: 8.2 Å), Mg^{2+} (8.6 Å), and Al^{3+} (9.5 Å) reached 86.3%, 98.0%, and 99.3%, respectively (Figure 8a, Table 3). Notably, the membrane also exhibited considerable rejection for monovalent ions (45.7% for K^+ and 47.0% for Na^+), despite their smaller hydrated diameters (Cl^-: 6.6 Å, K^+: 6.6 Å, Na^+: 7.2 Å) compared to the intrinsic pore size of UiO-66 (~6.0 Å). This

phenomenon is attributed to either ligand defects in the UiO-66 crystal structure [42] or dynamic ligand coordination behavior (e.g., carboxylate groups switching from edge-bridging to monodentate coordination) [128], which modulates the effective pore size and generates electrostatic interactions with ions. Cai et al. [91], optimized the membrane fabrication process and fabricated a thin, chemically stable, defect-minimized NH_2-UiO-66 membrane on carbon cloth via secondary growth. This membrane exhibited excellent separation performance in both aqueous and organic solvent systems, successfully rejecting various dyes (Figure 8c). Wang et al. [129] employed post-synthetic modification to repair ligand defects in UiO-66-$(OH)_2$ membranes, resulting in a high methyl blue rejection rate of 99.8% and an increased Na^+ rejection rate from 26% to 45% (Figure 8b, Table 3). Additionally, the UiO-66-NH_2@ZIF-8 composite membrane was reported to exhibit enhanced separation stability and performance for ion separation (Figure 8d) [97].

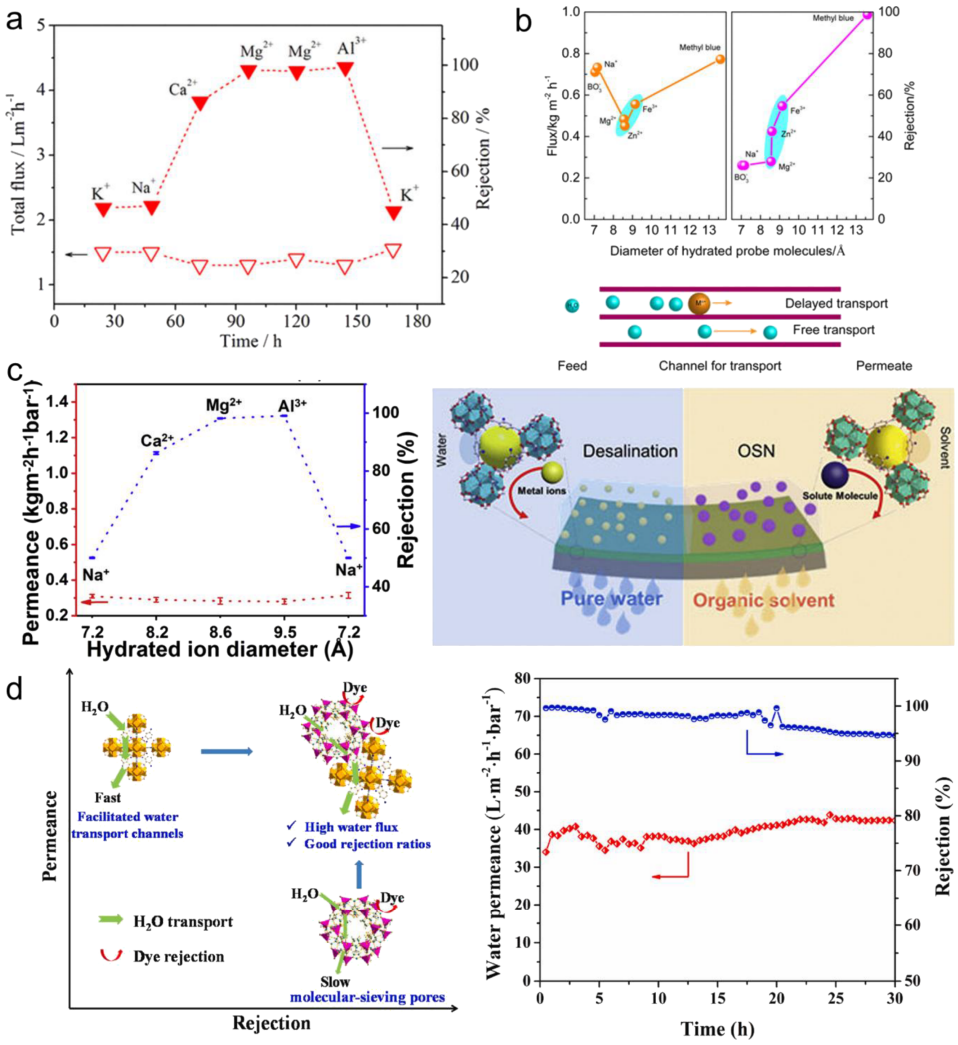

Figure 8. (**a**) Desalination performance of the UiO-66 membrane [45]. Copyright 2015, American Chemical Society. (**b**) Separation performance of UiO-66-$(OH)_2$ membranes before and after post-synthetic defect healing [129]. Copyright 2017, American Chemical Society. (**c**) Separation performance of the UiO-66(Zr)-NH_2 membrane [91]. Copyright 2020, Elsevier. (**d**) Separation mechanism and stability of the UiO-66-NH_2@ZIF-8 membrane [97]. Copyright 2022, Elsevier.

Table 3. Summary of the nanofiltration separation performance and the preparation methods of UiO-66-based membrane.

Membrane	Preparation Methods	Permeability (L m^{-2} h^{-1} bar^{-1})	Rejection	Ref.
UiO-66	*In-situ* growth	0.14	98.0% ($MgCl_2$)	[45]
UiO-66-NH_2	Secondary growth	0.17	99.8% (CH_2Cl_2)	[91]
UiO-66-NH_2@ZIF-8	Secondary growth	36.7	>97% (dye)	[97]
UiO-66	Counter-diffusion growth	~8	95% ($MgCl_2$)	[113]
UiO-66-$(OH)_2$	Secondary growth	0.8	74.9% (NaCl)	[129]
UiO-66-4F	Secondary growth	249.6	99.7% (dye)	[130]

3.3. Pervaporation

Pervaporation (PV) is a membrane separation technology that achieves mixture fractionation by exploiting differences in the solubility and diffusion coefficient of components within the membrane matrix. This low-energy-consumption technique is particularly suitable for separating azeotropic mixtures, near-boiling-point organic mixtures, trace water from organic solvents, trace organics from wastewater, and high-value organics from aqueous solutions [94,125,131–133]. Furthermore, PV can be integrated with chemical or biological reactions to enhance conversion efficiency by continuously removing reaction products. Recent studies have also explored the combination of PV with other separation technologies for water/organic separation, expanding its application potential in food processing, petrochemicals, pharmaceutical purification, and environmental protection.

Li et al. [87] utilized a high-quality, structurally stable UiO-66 membrane for PV desalination. Continuous operation tests under varying salt concentrations, feed temperatures, and harsh conditions systematically evaluated the membrane's performance for hypersaline water treatment. Experimental results demonstrated that the UiO-66 membrane achieved a high water flux of 37.4 $L \cdot m^{-2} \cdot h^{-1}$ with a salt rejection efficiency of up to 99.9%. Expanding upon this finding, Wang et al. [88] proposed a molecular-scale defect engineering strategy, wherein ligand vacancies were rationally tailored within the UiO-66 crystal lattice to construct a thin, robust, and high-performance missing-linker UiO-66 (ML-UiO-66) membrane for hypersaline seawater desalination. Under high-salinity conditions (35 $g \cdot L^{-1}$ NaCl), the ML-UiO-66 membrane maintained a stable flux of 29.8 $L \cdot m^{-2} \cdot h^{-1}$ alongside near-quantitative salt rejection. Mechanistically, the introduction of ligand defects modulated the hydrophilicity of sub-nanometer pore channels, thereby enhancing water diffusivity and facilitating rapid transmembrane water transport.

Liu et al. [49] validated the structural robustness of UiO-66 membranes for organic solvent dehydration: the membrane retained its structural integrity after exposure to boiling benzene and water, and its separation performance remained uncompromised even following the addition of sulfuric acid during a 200 h continuous stability test for water/n-butanol and water/furfural separation systems (Figure 9a). At 80 °C, the membrane delivered a water flux of up to 6.0 $kg \cdot m^{-2} \cdot h^{-1}$ with a separation factor exceeding 45,000, an order of magnitude (10–100) higher than commercial silica and polymer membranes with comparable flux, while exhibiting superior robustness under harsh operating environments relative to commercial NaA zeolite membranes. Huang et al. [53] prepared UiO-66 membranes through *in-situ* crystallization on micropatterned yttria-stabilized zirconia (YSZ) substrates for pervaporation (PV) applications. The micropatterned substrate design doubled the water flux of the UiO-66 membrane compared to conventional flat-substrate counterparts, while preserving a nearly constant separation factor (Figure 9b). Wu et al. [65]. developed a UiO-66-NH_2 membrane for PV desulfurization: for a thiophene/n-octane mixture at 40 °C, the membrane achieved a separation factor of 17.86 and a flux of 2.16 $kg \cdot m^{-2} \cdot h^{-1}$ (Table 4). Liu et al. [114] fine-tuned synthesis parameters to fabricate a well-intergrown UiO-66 membrane on a polymer substrate via interfacial diffusion growth, which was deployed for ethyl acetate dehydration (Figure 9c). This membrane featured fast, selective water transport pathways and an ethyl acetate/water separation factor of up to 7500 (Table 4).

Table 4. Summary of the pervaporation separation performance and the preparation methods of UiO-66-based membrane.

Membrane	Preparation Methods	Flux ($kg\ m^{-2}\ h^{-1}$)	Separation Factor	Feed Condition	Temp. (K)	Ref.
UiO-66	*In-situ* growth	0.64	4.3	10% EtOH/water	303	[125]
		1.49	4.9		323	
		3.15	4.8		343	
		1.58	5	10% MeOH/water	323	
		0.95	12.2	10% acetone/water	313	
		0.37	1.2	p-/m-xylene	313	
UiO-66-NH_2	Secondary growth	2.16	17.86	thiophene/n-octane	313	[65]
UiO-66	*In-situ* growth	2.96	1102	EtOH/water	313	[53]
UiO-66	Secondary growth	1.21	600	methanol/MTBE	313	[75]
UiO-66	Secondary growth	6.1	7500	methanol/MTBE	330	[114]
UiO-66	Secondary growth	37.4	>99.9%	H_2O/Salt	313	[90]
UiO-66-NH_2	Secondary growth	12.1	>99.7%	H_2O/Salt	363	[66]

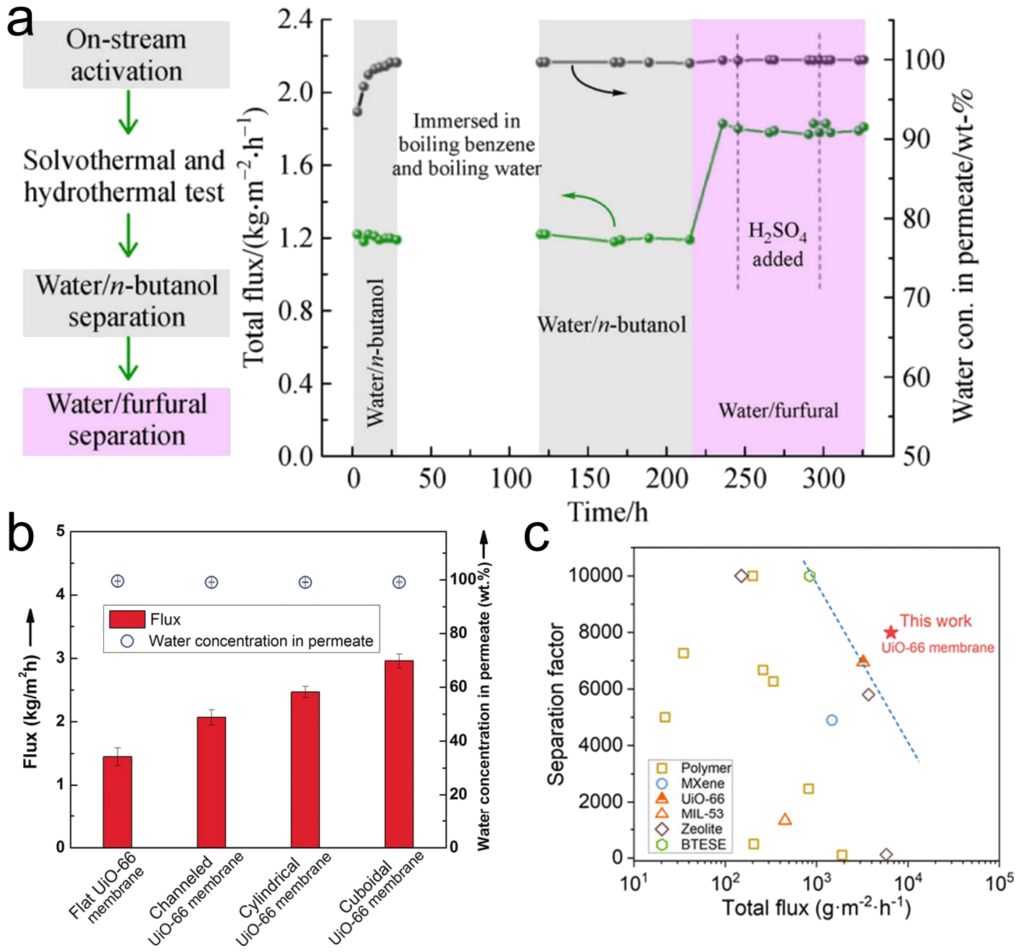

Figure 9. (**a**) Separation performance of UiO-66 membranes for n-butanol and furfural [49]. Copyright 2021, American Chemical Society. (**b**) Pervaporation performance of micropatterned UiO-66 membranes [53]. Copyright 2021, American Chemical Society. (**c**) Ethyl acetate/water separation performance of the UiO-66 membrane [114]. Copyright 2023, The Royal Society of Chemistry.

3.4. Ion Separation

Ion-selective separation is a critical application of membrane technology, with significant implications for lithium extraction from salt lakes, seawater desalination, high-salinity wastewater treatment, and salinity gradient energy generation [134–136]. UiO-66-based membranes achieve ion selectivity through the synergistic effect of size sieving (pore window size vs. ion hydrated diameter) and electrostatic interactions (functional groups vs. ion charge), enabling precise regulation of ion transport. The synergistic separation mechanism of "size sieving-electrostatic interaction" for UiO-66-based membranes essentially achieves the selective transport and rejection of target substances through the synergy between precise pore size matching (size sieving) and surface charge/affinity regulation (electrostatic interaction). This core foundation stems from the intrinsic structural characteristics of UiO-66: its face-centered cubic topological framework is composed of $Zr_6O_4(OH)_4$ clusters and organic ligands, with an intrinsic pore size of approximately 6.0 Å that can be tailored to the sub-nanometer (3–5 Å) via functional modification. Meanwhile, the functional groups of the ligands endow the membrane surface with controllable charge and specific affinity. The synergy of these two mechanisms is manifested as follows: size sieving first accomplishes preliminary separation and electrostatic interaction then enhances the transport or rejection of target substances, ultimately overcoming the performance bottlenecks of traditional single mechanisms. For example, when the $-NH_2$ modifies the UiO-66 framework via "ligand substitution", it primarily regulates the synergistic mechanism through two aspects-pore size reduction and polarity enhancement-with the core feature of stricter size sieving and more selective electrostatic interaction. The sulfonic acid group ($-SO_3H$) is a strongly acidic functional group; after modification, it modulates the synergistic mechanism through complete ionization to generate negative charges and slight pore size contraction, characterized by "electrostatic repulsion as the dominant effect and size sieving as the auxiliary separation role." Fluorine (-F) is the element with the highest electronegativity. After modification, it regulates the synergistic mechanism through precise pore size contraction and high-electronegativity dipole interactions, following the core logic that size sieving determines the upper limit of

selectivity, and ion-dipole interactions enhance transport efficiency, thus exhibiting the strongest synergy between the two mechanisms.

Zhang et al. [54] reported a UiO-66 membrane for rapid and selective transport of alkali metal ions: based on size sieving, the ion transport rate followed the order $Li^+ > Na^+ > K^+ > Rb^+$, with Li^+ preferentially transported. Lu et al. [64] developed an asymmetric UiO-66-$(COOH)_2$ membrane that mimics biological ion channels, featuring an ion-selective layer on one side and a nanoscale polymer region for rapid ion conduction on the other. I-V measurements showed that the currents of monovalent ions (K^+, Na^+, Li^+) through the sub-nanometer to nanoscale channels were three orders of magnitude higher than those of divalent ions (Ca^{2+}, Mg^{2+}) (Figure 10a), with a monovalent/divalent ion selectivity of 10^3. Furthermore, increasing the pH from 3 to 8 enhanced the monovalent/divalent ion selectivity by 10^2–10^4 times (Figure 10b, Table 5), attributed to the protonation/deprotonation of carboxyl groups regulating electrostatic repulsion.

Xu et al. [137] developed a lamellar UiO-66-NH_2 membrane on an anodized aluminum oxide (AAO) support via *in-situ* crystallization for metal ion separation. The lamellar architecture features nanoscale interlamellar gaps that enable efficient ion accessibility, while the intrinsic micropores of UiO-66-NH_2 crystals govern cation separation selectivity. This membrane achieved remarkable cation separation performance ($Na^+/Mg^{2+} > 200$, $Li^+/Mg^{2+} > 60$) alongside excellent operational stability over five consecutive electrodialysis cycles (Figure 10c). In a follow-up investigation, Xu et al. [138] constructed a lamellar UiO-66-SO_3H membrane on an AAO substrate through interfacial growth: the grafted sulfonic acid (-SO_3H) groups imparted a threefold enhancement in cation permeability compared to pristine UiO-66 membranes, while maintaining a Na^+/Mg^{2+} selectivity exceeding 140. Separately, Li et al. [113] reported sulfonated UiO-66-X membranes (X = SAG, NH-SAG, $(NH\text{-}SAG)_2$; SAG = sulfonic acid group) as biomimetic proton-conducting channels. Endowed with sub-1 nm pore windows and a high density of sulfonic acid moieties, these membranes mimicked the structure and function of natural proton channels, with ion conductivity following the order $H^+ > K^+ > Na^+ > Li^+$ (Figure 10d, Table 5). Notably, the UiO-66-$(NH\text{-}SAG)_2$ membrane exhibited ultrahigh proton selectivity (H^+/Li^+ up to 100, H^+/Na^+ ~80, H^+/K^+ ~70, Table 5), a threefold improvement relative to pristine UiO-66 membranes.

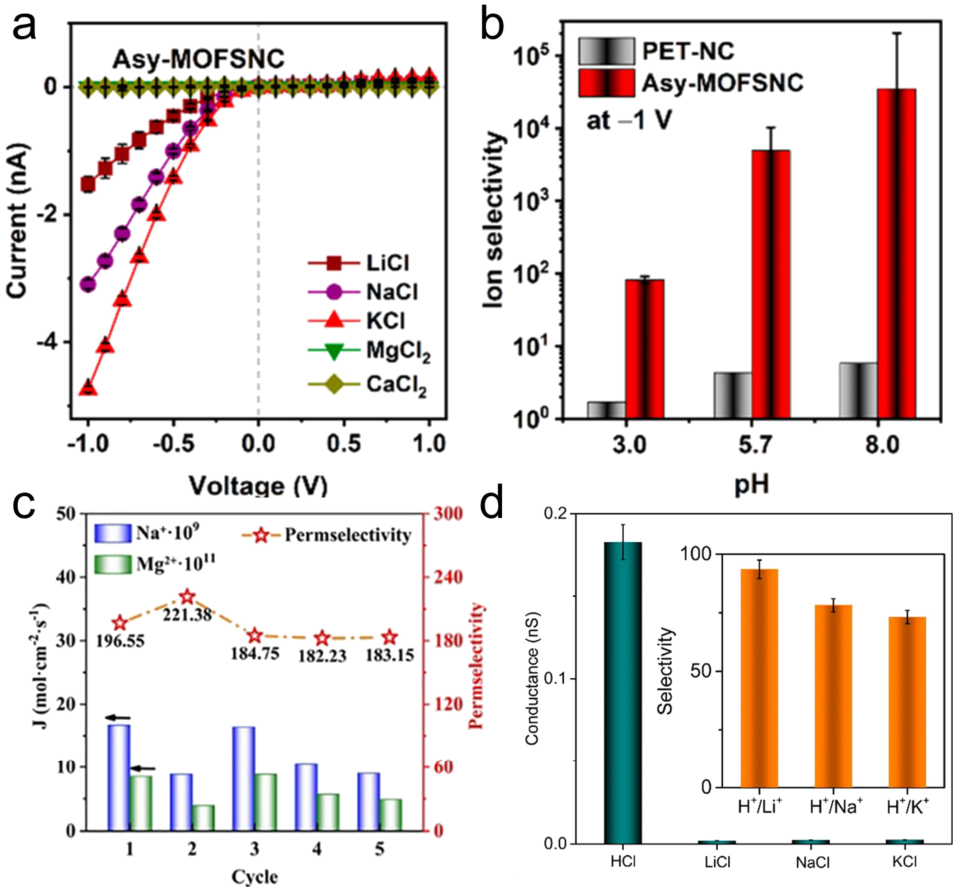

Figure 10. (**a**) I-V curves of UiO-66-$(COOH)_2$ membranes for different ions, (**b**) Effect f pH on monovalent/divalent ion selectivity of UiO-66-$(COOH)_2$ membranes [64]. Copyright 2016, Wiley-VCH. (**c**) Na^+/Mg^{2+} separation performance of lamellar UiO-66-NH_2 membranes over five electrodialysis cycles [137]. Copyright 2018, Wiley-VCH. (**d**) Ion conductivity of sulfonated UiO-66-X membranes [59]. Copyright 2020, Wiley-VCH.

Table 5. Summary of the ion separation performance and the preparation methods of UiO-66-based membrane.

Membrane	Preparation Methods	Permeability (Li^+ mol m^{-2} h^{-1})	Selectivity (Li^+/Mg^{2+})	Ref.
UiO-66@4.6%NTDS	Secondary growth	0.26	~46	[93]
ZIF-8/UiO-66-NH_2	Secondary growth	1.14	80 (Na^+/Li^+)	[95]
UiO-66	Electrochemical synthesis	11.2	286	[118]
UiO-66-4F	*In-situ* growth	0.19	134.8	[136]
UiO-66-X	Counter-diffusion growth	~10 S m^{-1} F^-	240 (F^-/Cl^-)	[137]
UiO-66-SO_3H (U-SM-0)	Secondary growth	7.56×10^{-2}	19	[138]
UiO-66-SO_3H (U-SM-10)		7.92×10^{-2}	4	
UiO-66-SO_3H (U-SM-25)		0.1	2	
UiO-66-NH_2 (LLM-1)	*In-situ* growth	4.5×10^{-2}	25	[139]
UiO-66-NH_2 (LLM-1)		4.32×10^{-2}	38	
UiO-66-NH_2 (LLM-1)		6.84×10^{-2}	37	
UiO-66-NH_2 (LLM-4)		7.2×10^{-2}	65	
HSO_3-UiO-66@QPPO-20%	*In-situ* growth	0.37	8.33	[140]
HSO_3-UiO-66@PVC	Secondary growth	8.84×10^{-3}	4.78	[141]
UiO-66-$(SH)_2$	Counter-diffusion growth	~11.8	1518	[142]

4. Conclusions

UiO-66 polycrystalline membranes have the inherent properties of zirconium-based metal-organic frameworks (MOFs), such as high chemical stability, tunable pore structure, and excellent adsorption and separation performance, while also incorporating the high efficiency and low energy consumption benefits of membrane separation technology, demonstrating outstanding separation potential in the field. In terms of preparation, both *in-situ* and secondary growth processes have been constantly refined, resulting in perfect control over membrane crystallinity and defect density. Seed-assisted secondary growth has become the most popular preparation method because of its ability to balance membrane uniformity and separation performance. In terms of applications, UiO-66 polycrystalline membranes have demonstrated a significant synergistic advantage in permeate flux and selectivity over traditional separation membranes in gas separation, nanofiltration, pervaporation, and ion separation, establishing a new paradigm for the separation of complex systems. However, the transition of UiO-66 polycrystalline membranes from laboratory research to industrial applications still confronts numerous hurdles, necessitating breakthroughs in critical restrictions such as large-scale preparation, performance stability, and application adaptability.

UiO-66 base membrane, relying on its precisely controllable pore structure, the synergistic separation mechanism of "size sieving-electrostatic interaction", and the specific affinity brought by functional modification, shows significant advantages and potential application value in the separation of complex systems. The pore size and surface affinity of UiO-66 can be accurately modified using ligand modification (the introduction of functional groups such as amino and carboxyl groups), mixed ligand methods, or metal node doping, resulting in bespoke membrane materials for effective separation. Furthermore, UiO-66 polycrystalline membranes overcome the limitations of traditional separation methods and are being expanded into emerging fields such as new energy (e.g., hydrogen purification, lithium-ion battery electrolyte purification), biomedicine (e.g., separation of biomacromolecules, drug purification), and environmental remediation (e.g., volatile organic compound (VOCs) recovery, seawater desalination) to fully explore their diverse application potential. Currently, research on UiO-66 polycrystalline membranes is primarily focused on laboratory-scale preparation. This approach is strongly reliant on small-area supports (such as ceramic tubes and porous glass), and its efficacy varies significantly from batch to batch. Uneven crystallization, increasing defect density, and high raw material prices (e.g., zirconium salts, organic ligands) continue to limit the practical applicability of large-area (square meter scale) membranes. Furthermore, imperfections in polycrystalline membranes, such as grain boundary gaps and pinholes, can easily cause "short-circuit permeation", which reduces separation selectivity. These flaws can develop, particularly under extreme separation conditions (e.g., high pressure, high temperature), compromising the membrane's long-term operating stability. Another significant concern is the weak interfacial interaction between the UiO-66 membrane and the support (e.g., polymers, inorganic substrates), which can cause the membrane layer to detach or peel off with prolonged use. In complicated separation systems with contaminants, high viscosity, or strong acids/bases (e.g., industrial organic wastewater, acidic gas separation), the UiO-66 membrane surface is prone to fouling and functional group degradation, resulting in reduced separation performance. As a result, the antifouling performance and chemical stability of UiO-66 membranes require further development.

Despite the huge potential for UiO-66-based membranes in new fields. In the biomedical field, surface biocompatibility must be enhanced in order to enable long-term in vivo membrane retention. To address industrial-scale production needs in the new energy field, large-area and low-defect preparation procedures for UiO-66-based membranes should be developed. Furthermore, a quantitative correlation model between membrane structure, application scenario, and performance requirements is required to guide the precision design of membrane materials. In the future, through the synergistic innovation of precision regulation of membrane properties via functional modification, enhancement of membrane mechanical/biological performance using composite substrates, and breakthroughs in large-scale preparation technologies, UiO-66-based membranes are expected to achieve the leap from laboratory-scale research to industrial-scale applications in the high-efficiency separation processes of the new energy industry chain.

To achieve large-scale fabrication of UiO-66 polycrystalline membranes, the following strategy is expected to be employed. Developing low-cost alternative raw materials (e.g., industrial-grade zirconium salts, renewable organic ligands); optimizing the concentration and temperature parameters of the reaction system to reduce energy consumption during the fabrication process; designing continuous fabrication equipment to achieve uniform fabrication of large-area membranes through online seed layer coating and continuous hydrothermal reaction. The zirconium oxychloride octahydrate ($ZrOCl_2 \cdot 8H_2O$) can be prioritized as the zirconium source, and its large-scale application can significantly reduce the cost of the metal precursor. In contrast to high-cost modulators such as benzoic acid and trifluoroacetic acid used in traditional synthesis, industrial-grade inorganic acids or organic acids can serve as cost-effective alternatives. Additionally, terephthalic acid derived from polyethylene terephthalate (PET) degradation is a viable ligand option for this process. Regarding the scale-up of the continuous crystallization reactor, the "multi-channel parallelization" strategy is adopted instead of enlarging the inner diameter of a single channel, which ensures uniform mass transfer during the large-scale production. Atomic layer deposition (ALD) was used to create a dense seed layer with minimal grain boundary gaps. Crosslinking agents (such as tetrabutyl titanate and silane coupling agents) were used to create a crosslinking network at the UiO-66 grain boundaries, which improved intergranular bonding and reduced defect development. Functional groups (such as hydroxyl and amino groups) were placed onto the support surface to improve chemical interaction between the membrane and the substrate. Intermediate transition layers (e.g., polydopamine coating, MOF-derived transition layers) were designed to compensate for changes in physical/chemical properties between the membrane and the support, decreasing the creation of dead-end layers at the interface. A hierarchical pore structure design was employed to create an UiO-66 micro-mesoporous composite structure, in which mesoporous channels lower permeation resistance while the microporous framework ensures separation selectivity. Targeted specific affinity functional groups were introduced via ligand modification, and pore size was altered via metal node replacement (e.g., partial substitution of Zr^{4+} with Ti^{4+} or Hf^{4+}), enhancing both permeability and selectivity.

Author Contributions

S.S.: writing— reviewing and editing; Y.Z.: visualization, methodology; M.W.: conceptualization, writing—reviewing and editing; R.H.: writing—original draft preparation, Z.J.: data curation, Y.Z.: visualization, S.C.: writing—original draft preparation, reviewing and editing, funding acquisition. All authors have read and agreed to the published version of the manuscript.

Funding

This research was financially funded by the National Natural Science Foundation of China (No. 22378412), Yangzhou "Green Yang Jinfeng Plan" excellent doctor talent funding program and Yangzhou University Startup Fund for Distinguished Scholars (137013525).

Institutional Review Board Statement

Not applicable.

Informed Consent Statement

Not applicable.

Data Availability Statement

Data will be made available on request.

Conflicts of Interest

The authors declare no conflict of interest.

Use of AI and AI-Assisted Technologies

No AI tools were utilized for this paper.

References

1. Sholl, D.S.; Lively, R.P. Seven chemical separations to change the world. *Nature* **2016**, *532*, 435–437.
2. Kolle, J.M.; Fayaz, M.; Sayari, A. Understanding the effect of water on CO_2 adsorption. *Chem. Rev.* **2021**, *121*, 7280–7345.
3. Shi, Y.; Liang, B.; Lin, R.-B.; et al. Gas separation via hybrid metal-organic framework/polymer membranes. *Trends Chem.* **2020**, *2*, 254–269.
4. Shih, C.F.; Zhang, T.; Li, J.; et al. Powering the future with liquid sunshine. *Joule* **2018**, *2*, 1925–1949.
5. Linnhoff, B.; Dunford, H.; Smith, R. Heat integration of distillation columns into overall processes. *Chem. Eng. Sci.* **1983**, *38*, 1175–1188.
6. Koros, W.J.; Lively, R.P. Water and beyond: Expanding the spectrum of large-scale energy efficient separation processes. *AIChE J.* **2012**, *58*, 2624.
7. Cheng, Y.; Datta, S.J.; Zhou, S.; et al. Advances in metal-organic framework-based membranes. *Chem. Soc. Rev.* **2022**, *51*, 8300–8350.
8. Qian, Q.; Asinger, P.A.; Lee, M.J.; et al. MOF-based membranes for gas separations. *Chem. Rev.* **2020**, *120*, 8161–8266.
9. Yang, Z.; Wu, Z.; Peh, S.B.; et al. Mixed-matrix membranes containing porous materials for gas separation: From metal–organic frameworks to discrete molecular cages. *Engineering* **2023**, *23*, 40–55.
10. Zhang, Y.; Yin, B.H.; Huang, L.; et al. MOF membranes for gas separations. *Prog. Mater. Sci.* **2025**, *151*, 101432.
11. Fei, L.; Chen, C.; Xu, J.; et al. Biomineralized metal-organic framework membrane with high-crystallinity for ultrafast molecular separation. *J. Membr. Sci.* **2025**, *717*, 123569.
12. Zhang, Z.; Yang, Z.; Li, S.; et al. Hot solution strategy to prepare Zr-MOF/polyimide mixed matrix membranes for high-performance helium separation. *J. Membr. Sci.* **2025**, *729*, 124137.
13. Baker, R.W. Future Directions of Membrane Gas Separation Technology. *Ind. Eng. Chem. Res.* **2002**, *41*, 1393–1411.
14. Park, H.B.; Kamcev, J.; Robeson, L.M.; et al. Maximizing the right stuff: The trade-off between membrane permeability and selectivity. *Science* **2017**, *356*, eaab0530.
15. Cheng, S.-Q.; Liu, Y.; Sun, Y. Macrocycle-based metal-organic and covalent organic framework membranes. *Coord. Chem. Rev.* **2025**, *534*, 216559.
16. Caro, J.; Noack, M. Zeolite membranes-Recent developments and progress. *Microporous Mesoporous Mater.* **2008**, *115*, 215–233.
17. Trickett, C.A.; Helal, A.; Al-Maythalony, B.A.; et al. The chemistry of metal-organic frameworks for CO_2 capture, regeneration and conversion. *Nat. Rev. Mater.* **2017**, *2*, 17045.
18. Kalmutzki, M.J.; Hanikel, N.; Yaghi, O.M. Secondary building units as the turning point in the development of the reticular chemistry of MOFs. *Sci. Adv.* **2018**, *4*, eaat9180.
19. Qiu, S.; Xue, M.; Zhu, G. Metal-organic framework membranes: From synthesis to separation application. *Chem Soc Rev* **2014**, *43*, 6116–6140.
20. Kang, Z.; Guo, H.; Fan, L.; et al. Scalable crystalline porous membranes: Current state and perspectives. *Chem. Soc. Rev.* **2021**, *50*, 1913–1944.
21. Macreadie, L.K.; Idrees, K.B.; Smoljan, C.S.; et al. Expanding Linker Dimensionality in Metal-organic Frameworks for sub-Angstrom Pore Control for Separation Applications. *Angew. Chem. Int. Ed.* **2023**, *62*, e202304094.
22. Wu, T.; Prasetya, N.; Li, K. Recent advances in aluminium-based metal-organic frameworks (MOF) and its membrane applications. *J. Membr. Sci.* **2020**, *615*, 118493.
23. Liang, W.; Bhatt, P.M.; Shkurenko, A.; et al. A Tailor-Made Interpenetrated MOF with Exceptional Carbon-Capture Performance from Flue Gas. *Chem* **2019**, *5*, 950–963.
24. Qiu, Z.; Zhang, S.; Lin, H.; et al. Controllable etching construction of nickel-based Prussian blue analog nanocages for stabilized energy storage in aqueous nickel-zinc batteries. *Green Chem. Eng.* **2025**.
25. Li, H.-Y.; Zhao, S.-N.; Zang, S.-Q.; et al. Functional metal–organic frameworks as effective sensors of gases and volatile compounds. *Chem. Soc. Rev.* **2020**, *49*, 6364–6401.
26. Khafaga, D.S.; El-Morsy, M.T.; Faried, H.; et al. Metal–organic frameworks in drug delivery: Engineering versatile platforms for therapeutic applications. *RSC Adv.* **2024**, *14*, 30201–30229.
27. Knebel, A.; Caro, J. Metal-organic frameworks and covalent organic frameworks as disruptive membrane materials for energy-efficient gas separation. *Nat. Nanotechnol.* **2022**, *17*, 911–923.

28. Hermes, S.; Schröder, F.; Chelmowski, R.; et al. Selective nucleation and growth of metal-rganic open framework thin films on patterned COOH/CF_3-terminated self-assembled monolayers on Au (111). *J. Am. Chem. Soc.* **2005**, *127*, 13744–13745.
29. Arnold, M.; Kortunov, P.; Jones, D.J.; et al. *Oriented Crystallisation on Supports and Anisotropic Mass Transport of the Metal-Organic Framework Manganese Formate*. *Eur.J.Inorg.Chem*. **2007**, 1, 60-64.
30. Biemmi, E.; Scherb, C.; Bein, T. Oriented growth of the metal organic framework $Cu_3(BTC)_2(H_2O)_3 \cdot xH_2O$ tunable with functionalized self-assembled monolayers. *J. Am. Chem. Soc.* **2007**, *129*, 8054–8055.
31. Scherb, C.; Schödel, A.; Bein, T. Directing the structure of metal-organic frameworks by oriented surface growth on an organic monolayer. *Angew. Chem. Int. Ed.* **2008**, *47*, 5777–5779.
32. Gascon, J.; Aguado, S.; Kapteijn, F. Manufacture of dense coatings of $Cu_3(BTC)_2$ (HKUST-1) on α-alumina. *Microporous Mesoporous Mater.* **2008**, *113*, 132–138.
33. Zou, X.; Zhu, G.; Hewitt, I.J.; et al. Synthesis of a metal-organic framework film by direct conversion technique for VOCs sensing. *Dalton Trans.* **2009**, 3009–3013.
34. Liu, J.; Sun, F.; Zhang, F.; et al. In situ growth of continuous thin metal-organic framework film for capacitive humidity sensing. *J. Mater. Chem.* **2011**, *21*, 3775–3778.
35. Liu, Y.; Ng, Z.; Khan, E.A.; et al. Synthesis of continuous MOF-5 membranes on porous α-alumina substrates. *Microporous Mesoporous Mater.* **2009**, *118*, 296–301.
36. Guo, H.; Zhu, G.; Hewitt, I.J.; et al. "Twin copper source" growth of metal− organic framework membrane: $Cu_3(BTC)_2$ with high permeability and selectivity for recycling H_2. *J. Am. Chem. Soc.* **2009**, *131*, 1646–1647.
37. Wang, C.; Liu, X.; Demir, N.K.; et al. Applications of water stable metal-organic frameworks. *Chem Soc Rev* **2016**, *45*, 5107–5134.
38. Liu, G.; Chemikova, V.; Liu, Y.; et al. Mixed matrix formulations with MOF molecular sieving for key energy-intensive separations. *Nat. Mater.* **2019**, *17*, 283–289.
39. Liu, X.; Wang, X.; Kapteijn, F.; et al. Water and metal-organic frameworks: From interaction toward utilization. *Chem. Rev.* **2020**, *120*, 8303–8377.
40. Cavka, J.H.; Jakobsen, S.; Olsbye, U.; et al. A new zirconium inorganic building brick forming metal organic frameworks with exceptional stability. *J. Am. Chem. Soc.* **2008**, *130*, 13850–13851.
41. Pearson, R.G. Hard and soft acids and bases. *J. Am. Chem. Soc.* **1963**, *85*, 3533–3539.
42. Valenzano, L.; Civalleri, B.; Chavan, S.; et al. Disclosing the complex structure of UiO-66 metal organic framework: A synergic combination of experiment and theory. *Chem. Mater.* **2011**, *23*, 1700–1718.
43. Feng, L.; Pang, J.; She, P.; et al. Metal-organic frameworks based on group 3 and 4 metals. *Adv. Mater.* **2020**, *32*, e2004414.
44. Bai, Y.; Dou, Y.; Xie, L.-H.; et al. Zr-based metal-organic frameworks: Design, synthesis, structure, and applications. *Chem. Soc. Rev.* **2016**, *45*, 2327–2367.
45. Liu, X.; Demir, N.K.; Wu, Z.; et al. Highly Water-Stable Zirconium Metal-Organic Framework UiO-66 Membranes Supported on Alumina Hollow Fibers for Desalination. *J. Am. Chem. Soc.* **2015**, *137*, 6999–7002.
46. Hu, Z.; Zhao, D. De facto methodologies toward the synthesis and scale-up production of UiO-66-type metal-organic frameworks and membrane materials. *Dalton Trans.* **2015**, *44*, 19018–19040.
47. Liu, X. Metal-organic framework UiO-66 membranes. *Front. Chem. Sci.* **2020**, *14*, 216–232.
48. Ghalei, B.; Wakimoto, K.; Wu, C.Y.; et al. Rational tuning of zirconium metal-organic framework membranes for hydrogen purification. *Angew. Chem. Int. Ed.* **2019**, *58*, 19034–19040.
49. Liu, X.; Wang, C.; Wang, B.; et al. Novel organic-dehydration membranes prepared from zirconium metal-organic frameworks. *Adv. Funct. Mater.* **2017**, *27*, 1604311.
50. Kim, J.Y.; Barcus, K.; Cohen, S.M. Controlled two-dimensional alignment of metal-organic frameworks in polymer films. *J. Am. Chem. Soc.* **2021**, *143*, 3703–3706.
51. Lee, S.; Yaghi, O.M. 'Eye'of the molecule-a viewpoint. *Faraday Discuss.* **2021**, *231*, 145–149.
52. Liu, H.; Gao, J.; Liu, G.; et al. Enhancing permeability of thin film nanocomposite membranes via covalent linking of polyamide with the incorporated metal-organic frameworks. *Ind. Eng. Chem. Res.* **2019**, *58*, 8772–8783.
53. Huang, K.; Wang, B.; Guo, S.; et al. Micropatterned ultrathin MOF membranes with enhanced molecular sieving property. *Angew. Chem. Int. Ed.* **2018**, *57*, 13892–13896.
54. Zhang, H.; Hou, J.; Hu, Y.; et al. Ultrafast selective transport of alkali metal ions in metal organic frameworks with subnanometer pores. *Sci. Adv.* **2018**, *4*, eaaq0066.
55. Liu, J.; Canfield, N.; Liu, W. Preparation and characterization of a hydrophobic metal-organic framework membrane supported on a thin porous metal sheet. *Ind. Eng. Chem. Res.* **2016**, *55*, 3823–3832.
56. Shan, B.; James, J.B.; Armstrong, M.R.; et al. Influences of deprotonation and modulation on nucleation and growth of UiO-66: Intergrowth and Orientation. *J. Phys. Chem. C* **2018**, *122*, 2200–2206.

57. Luo, C.; Cong, S.; Luan, L.; et al. High performance MOF UiO-66 membranes for MeOH/MTBE separation. *J. Membr. Sci.* **2024**, *693*, 122335.
58. Li, W.; Su, P.; Li, Z.; et al. Ultrathin metal-organic framework membrane production by gel-vapour deposition. *Nat. Commun.* **2017**, *8*, 406.
59. Ma, X.; Wan, Z.; Li, Y.; et al. Anisotropic gas separation in oriented ZIF-95 membranes prepared by vapor-assisted in-plane epitaxial growth. *Angew. Chem. Int. Ed.* **2020**, *59*, 20858–20862.
60. Huang, K.; Li, Q.; Liu, G.; et al. A ZIF-71 hollow fiber membrane fabricated by contra-diffusion. *ACS Appl. Mater. Interfaces* **2015**, *7*, 16157–16160.
61. Zhou, S.; Shekhah, O.; Jia, J.; et al. Electrochemical synthesis of continuous metal-organic framework membranes for separation of hydrocarbons. *Nat. Energy* **2021**, *6*, 882–891.
62. Zhou, S.; Wei, Y.; Zhuang, L.; et al. Introduction of metal precursors by electrodeposition for the *in situ* growth of metal-organic framework membranes on porous metal substrates. *J. Mater. Chem. A* **2017**, *5*, 1948–1951.
63. Wu, W.; Fan, J.; Wang, D.; et al. Ultrathin UiO-66-NH_2 polycrystalline membrane for CO_2/CH_4 separation. *Carbon Capture Sci. Technol.* **2024**, *11*, 100183.
64. Lu, J.; Zhang, H.; Hou, J.; et al. Efficient metal ion sieving in rectifying subnanochannels enabled by metal-organic frameworks. *Nat. Mater.* **2020**, *19*, 767–774.
65. Wu, F.; Cao, Y.; Liu, H.; et al. High-performance UiO-66-NH_2 tubular membranes by zirconia-induced synthesis for desulfurization of model gasoline via pervaporation. *J. Membr. Sci.* **2018**, *556*, 54–65.
66. Wan, L.; Zhou, C.; Xu, K.; et al. Synthesis of highly stable UiO-66-NH_2 membranes with high ions rejection for seawater desalination. *Microporous Mesoporous Mater.* **2017**, *252*, 207–213.
67. Huang, A.; Bux, H.; Steinbach, F.; et al. Molecular-sieve membrane with hydrogen permselectivity: ZIF-22 in LTA topology prepared with 3-aminopropyltriethoxysilane as covalent linker. *Angew. Chem.* **2010**, *122*, 5078–5081.
68. Zhang, Y.; Zhao, J.; Wang, K.; et al. Green Synthesis of Acid-Base Bi-functional UiO-66-Type Metal-Organic Frameworks Membranes Supported on Polyurethane Foam for Glucose Conversion. *ChemistrySelect* **2018**, *3*, 9378–9387.
69. Liang, H.; Jiao, X.; Li, C.; et al. Flexible self-supported metal-organic framework mats with exceptionally high porosity for enhanced separation and catalysis. *J. Mater. Chem. A* **2018**, *6*, 334–341.
70. Zhang, C.; Zhao, Y.; Li, Y.; et al. Defect-controlled preparation of UiO-66 metal-organic framework thin films with molecular sieving capability. *Chem. Asian J.* **2016**, *11*, 207–210.
71. Lu, A.X.; Ploskonka, A.M.; Tovar, T.M.; et al. Direct surface growth of UiO-66-NH_2 on polyacrylonitrile nanofibers for efficient toxic chemical removal. *Ind. Eng. Chem. Res.* **2017**, *56*, 14502–14506.
72. Betke, U.; Proemmel, S.; Rannabauer, S.; et al. Silane functionalized open-celled ceramic foams as support structure in metal organic framework composite materials. *Microporous Mesoporous Mater.* **2017**, *239*, 209–220.
73. Snyder, M.A.; Tsapatsis, M. Hierarchical nanomanufacturing: From shaped zeolite nanoparticles to high-performance separation membranes. *Angew. Chem. Int. Ed.* **2007**, *46*, 7560–7573.
74. Sun, Y.; Yan, J.; Gao, Y.; et al. Fabrication of highly oriented ultrathin zirconium metal-organic framework membrane from nanosheets towards unprecedented gas separation. *Angew. Chem. Int. Ed.* **2023**, *62*, e202216697.
75. Wu, F.; Lin, L.; Liu, H.; et al. Synthesis of stable UiO-66 membranes for pervaporation separation of methanol/methyl tert-butyl ether mixtures by secondary growth. *J. Membr. Sci.* **2017**, *544*, 342–350.
76. Schaate, A.; Roy, P.; Godt, A.; et al. Modulated synthesis of Zr-based metal-organic frameworks: From nano to single crystals. *Chem. A Eur. J.* **2011**, *17*, 6643–6651.
77. Piszczek, P.; Radtke, A.; Grodzicki, A.; et al. The new type of $[Zr_6(\mu_3\text{-}O)_4(\mu_3\text{-}OH)_4]$ cluster core: Crystal structure and spectral characterization of $[Zr_6O_4(OH)_4(OOCR)_{12}]$(R= But, $C(CH_3)_2Et$). *Polyhedron* **2007**, *26*, 679–685.
78. Yao, H.-B.; Yan, Y.-X.; Gao, H.-L.; et al. An investigation of zirconium (IV)-glycine (CP-2) hybrid complex in bovine serum albumin protein matrix under varying conditions. *J. Mater. Chem.* **2011**, *21*, 19005–19012.
79. Yan, J.; Sun, Y.; Ji, T.; et al. Room-temperature synthesis of defect-engineered Zirconium-MOF membrane enabling superior CO_2/N_2 selectivity with zirconium-oxo cluster source. *J. Membr. Sci.* **2022**, *653*, 120496.
80. Yan, J.; Ji, T.; Sun, Y.; et al. Room temperature fabrication of oriented Zr-MOF membrane with superior gas selectivity with zirconium-oxo cluster source. *J. Membr. Sci.* **2022**, *661*, 120959.
81. Yan, J.; Sun, Y.; Ji, T.; et al. Facile synthesis of oriented Zr-MOF membrane under complete room-temperature condition with superb selectivity for carbon capture. *Ind. Eng. Chem. Res.* **2023**, *62*, 5973–5983.
82. Friebe, S.; Geppert, B.; Steinbach, F.; et al. Metal-organic framework UiO-66 layer: A highly oriented membrane with good selectivity and hydrogen permeance. *ACS Appl. Mater. Interfaces* **2017**, *9*, 12878–12885.
83. Van der Drift, A. Evolutionary selection, a principle governing growth orientation in vapour-deposited layers. *Philips Res. Rep* **1967**, *22*, 267.

84. Sun, Y.; Song, C.; Guo, X.; et al. Concurrent manipulation of out-of-plane and regional in-plane orientations of NH_2-UiO-66 membranes with significantly reduced anisotropic grain boundary and superior H_2/CO_2 separation performance. *ACS Appl. Mater. Interfaces* **2019**, *12*, 4494–4500.
85. Yan, J.; Sun, Y.; Ji, T.; et al. Cooperative defect tailoring: A promising protocol for exceeding performance limits of state-of-the-art MOF membranes. *J. Membr. Sci.* **2021**, *635*, 119515.
86. Rong, R.; Sun, Y.; Ji, T.; et al. Fabrication of highly CO_2/N_2 selective polycrystalline UiO-66 membrane with two-dimensional transition metal dichalcogenides as zirconium source via tertiary solvothermal growth. *J. Membr. Sci.* **2020**, *610*, 118275.
87. Li, H.; Fu, M.; Wang, S.Q.; et al. Stable Zr-based metal-organic framework nanoporous membrane for efficient desalination of hypersaline water. *Environ. Sci. Technol.* **2021**, *55*, 14917–14927.
88. Wang, X.; Lyu, Q.; Tong, T.; et al. Robust ultrathin nanoporous MOF membrane with intra-crystalline defects for fast water transport. *Nat. Commun.* **2022**, *13*, 266.
89. Zhang, Y.; Sun, S.; Wang, M.; et al. Metal-organic framework (MOF) membranes for Mg^{2+}/Li^{+} separation. *Sep. Sci. Technol.* **2025**, *374,* 133737.
90. Miyamoto, M.; Kohmura, S.; Iwatsuka, H.; et al. In situ solvothermal growth of highly oriented Zr-based metal organic framework UiO-66 film with monocrystalline layer. C*rystEngComm* **2015**, *17,* 3422-3425.
91. Cai, Y.; Shi, D.; Liu, G.; et al. Polycrystalline zirconium metal-organic framework membranes supported on flexible carbon cloth for organic solvent nanofiltration. *J. Membr. Sci.* **2020**, *615*, 118551.
92. Xu, T.; Wu, B.; Li, W.; et al. Perfect confinement of crown ethers in MOF membrane for complete dehydration and fast transport of monovalent ions. *Sci. Adv.* **2024**, *10*, eadn0944.
93. Li, W.; Xu, T.; Sheng, F.; et al. UiO-66 membranes with confined naphthalene disulfonic acid for selective monovalent ion separation. *J. Membr. Sci.* **2024**, *703*, 122829.
94. Peng, P.; Shi, B.; Lan, Y. Preparation of PDMS-silica nanocomposite membranes with silane coupling for recovering ethanol by pervaporation. *Sep. Sci. Technol.* **2011**, *46*, 420–427.
95. Abdollahzadeh, M.; Chai, M.; Hosseini, E.; et al. Designing angstrom-scale asymmetric MOF-on-MOF cavities for high monovalent ion selectivity. *Adv. Mater.* **2022**, *34*, e2107878.
96. Das, S.; Ben, T. A [COF-300]-[UiO-66] composite membrane with remarkably high permeability and H_2/CO_2 separation selectivity. *Dalton Trans* **2018**, *47*, 7206–7212.
97. Xu, Y.; Zhao, X.; Chang, R.; et al. Designing heterogeneous MOF-on-MOF membrane with hierarchical pores for effective water treatment. *J. Membr. Sci.* **2022**, *658*, 120737.
98. Mo, R.J.; Chen, S.; Huang, L.Q.; et al. Regulating ion affinity and dehydration of metal-organic framework sub-nanochannels for high-precision ion separation. *Nat. Commun.* **2024**, *15*, 2145.
99. Guo, H.; Liu, J.; Li, Y.; et al. Post-synthetic modification of highly stable UiO-66-NH_2 membranes on porous ceramic tubes with enhanced H_2 separation. *Microporous Mesoporous Mater.* **2021**, *313*, 110823.
100. Wu, L.; Liang, Y.; Zhang, B.; et al. Post-synthetic modification of MOF UiO-66-NH_2 membranes for efficient methanol/organic separation. *J. Membr. Sci.* **2025**, *715*, 123475.
101. Xiao, H.; Chai, M.; Hosseini, A.; et al. UiO-66-$(COONa)_2$ membrane with programmable ionic channels for lithium ion-selective transport. *J. Membr. Sci.* **2023**, *670*, 121312.
102. Liu, Y.; Liu, L.; Yang, Y.; et al. Salicylaldehyde-assisted ZrO_2-induced conversion approach to prepare high performance hollow fiber-supported UiO-66-NH_2 membrane for hydrogen separation. *J. Membr. Sci.* **2023**, *684*, 121851.
103. Li, P.; Sun, Y.; Zhang, Z.; et al. Preparation of UiO-66 membrane through heterogeneous nucleation assisted growth strategy for efficient CO_2 capture under humid conditions. *Sep. Purif. Technol.* **2024**, *351*, 128067.
104. Miikkulainen, V.; Leskelae, M.; Ritala, M.; et al. Crystallinity of inorganic films grown by atomic layer deposition: Overview and general trends. *J. Appl. Phys.* **2013**, *113*, 430.
105. Ma, X.; Kumar, P.; Mittal, N.; et al. Zeolitic imidazolate framework membranes made by ligand-induced permselectivation. *Science* **2018**, *361*, 1008–1011.
106. Lausund, K.B.; Nilsen, O. All-gas-phase synthesis of UiO-66 through modulated atomic layer deposition. *Nat. Commun.* **2016**, *7*, 13578.
107. Lausund, K.B.; Petrovic, V.; Nilsen, O. All-gas-phase synthesis of amino-functionalized UiO-66 thin films. *Dalton Trans.* **2017**, *46*, 16983–16992.
108. Virmani, E.; Rotter, J.M.; Mähringer, A.; et al. On-surface synthesis of highly oriented thin metal-organic framework films through vapor-assisted conversion. *J. Am. Chem. Soc.* **2018**, *140*, 4812.
109. Eum, K.; Rownaghi, A.; Choi, D.; et al. Fluidic processing of high-performance ZIF-8 membranes on polymeric hollow fibers: Mechanistic insights and microstructure control. *Adv. Funct. Mater.* **2016**, *26*, 5011–5018.
110. Brown, A.J.; Brunelli, N.A.; Eum, K.; et al. Interfacial microfluidic processing of metal-organic framework hollow fiber membranes. *Science* **2014**, *345*, 72–75.

111. Sun, Y.; Yan, J.; Jiang, J.; et al. Hierarchical defect-rich UiO-66 membrane towards superior flue gas and butane isomer separations. *Sci. Bull.* **2024**, *69*, 2174–2178.
112. Liu, G.; Guo, Y.; Chen, C.; et al. Eliminating lattice defects in metal-organic framework molecular-sieving membranes. *Nat. Mater.* **2023**, *22*, 769–776.
113. Liu, G.; Mo, B.; Guo, Y.; et al. Confined-Coordination Induced Intergrowth of Metal-Organic Frameworks into Precise Molecular Sieving Membranes. *Angew. Chem. Int. Ed.* **2024**, *63*, e202405676.
114. Liu, G.; Wang, Z.; Chen, C.; et al. Zr-MOF membranes with ultra-fast water-selective permeation towards intensification of esterification reaction. *Chem. Commun.* **2023**, *59*, 8075–8078.
115. Falcaro, P.; Ricco, R.; Doherty, C.M.; et al. MOF positioning technology and device fabrication. *Chem. Soc. Rev.* **2014**, *43*, 5513–5560.
116. Ameloot, R.; Stappers, L.; Fransaer, J.; et al. Patterned growth of metal-organic framework coatings by electrochemical synthesis. *Chem. Mater.* **2009**, *21*, 2580–2582.
117. Hou, Q.; Wu, Y.; Zhou, S.; et al. Ultra-tuning of the aperture size in stiffened ZIF-8_Cm frameworks with mixed-linker strategy for enhanced CO_2/CH_4 separation. *Angew. Chem. Int. Ed.* **2019**, *58*, 327–331.
118. Xie, S.; Monnens, W.; Zhang, W.; et al. Control over cathodic deposition of continuous UiO-66 films for ion-selective transport. *Cell Rep. Phys. Sci.* **2023**, *4*, 101412.
119. Stassen, I.; Styles, M.; Van Assche, T.; et al. Electrochemical film deposition of the zirconium metal-organic framework UiO-66 and application in a miniaturized sorbent trap. *Chem. Mater.* **2015**, *27*, 1801–1807.
120. Hod, I.; Karlin, D.M.; Deria, P.; et al. Directed growth of electroactive metal-organic framework thin films using electrophoretic deposition. *Adv. Mater.* **2014**, *26*, 6295–6300.
121. Zhang, X.; Wang, H.; Wang, Q.; et al. Electrochemical versatility synthesis of functional UiO-66 series heterogeneous membranes for highly efficient salinity gradient energy harvesting. *Chem. Eng. J.* **2025**, *506*, 159847.
122. Wang, Y.; Jiang, H.; Guo, Z.; et al. Advances in organic microporous membranes for CO_2 separation. *Energy Environ. Sci.* **2023**, *16*, 53-75.
123. Wu, W.; Li, Z.; Chen, Y.; et al. Polydopamine-modified metal-organic framework membrane with enhanced selectivity for carbon capture. *Environ. Sci. Technol.* **2019**, *53*, 3764–3772.
124. Das, S.; Ben, T.; Qiu, S.; et al. Two-Dimensional COF-Three-Dimensional MOF Dual-Layer Membranes with Unprecedentedly High H_2/CO_2 Selectivity and Ultrahigh Gas Permeabilities. *ACS Appl. Mater. Interfaces* **2020**, *12*, 52899–52907.
125. Miyamoto, M.; Hori, K.; Goshima, T.; et al. An organoselective zirconium-based metal-organic-framework UiO-66 membrane for pervaporation. *Eur. J. Inorg. Chem.* **2017**, *2017*, 2094–2099.
126. Cui, X.; Kong, G.; Feng, Y.; et al. Interfacial polymerization of MOF “monomers” to fabricate flexible and thin membranes for molecular separation with ultrafast water transport. *J. Mater. Chem. A* **2021**, *9*, 17528–17537.
127. Liu, Y.-C.; Yeh, L.-H.; Zheng, M.-J.; et al. Highly selective and high-performance osmotic power generators in subnanochannel membranes enabled by metal-organic frameworks. *Sci. Adv.* **2021**, *7*, eabe9924.
128. Devautour-Vinot, S.; Martineau, C.; Diaby, S.; et al. Caffeine confinement into a series of functionalized porous zirconium MOFs: A joint experimental/modeling exploration. *J. Phys. Chem. C* **2013**, *117*, 11694–11704.
129. Wang, X.; Zhai, L.; Wang, Y.; et al. Improving water-treatment performance of zirconium metal-organic framework membranes by postsynthetic defect healing. *ACS Appl. Mater. Interfaces* **2017**, *9*, 37848–37855.
130. Wu, H.; Si, Z.; Zhang, J.; et al. Fabrication of antifouling UiO-66 nanofiltration membranes via surface fluorination engineering. *Desalination* **2023**, *567*, 116957.
131. Zhang, W.-d.; Sun, W.; Yang, J.; et al. The Study on Pervaporation Behaviors of Dilute Organic Solution Through PDMS/PTFE Composite Membrane. *Appl. Biochem. Biotechnol.* **2010**, *160*, 156–167.
132. Smitha, B.; Suhanya, D.; Sridhar, S.; et al. Separation of organic-organic mixtures by pervaporation-a review. *J. Membr. Sci.* **2004**, *241*, 1–21.
133. Pivovar, B.S.; Wang, Y.; Cussler, E.L. Pervaporation membranes in direct methanol fuel cells. *J. Membr. Sci.* **1999**, *154*, 155–162.
134. Li, X.; Zhang, H.; Wang, P.; et al. Fast and selective fluoride ion conduction in sub-1-nanometer metal-organic framework channels. *Nat. Commun.* **2019**, *10*, 2490.
135. Lu, J.; Hu, X.; Ung, K.M.; et al. Metal-organic frameworks as a subnanometer platform for ion-ion selectivity. *Acc. Mater. Res.* **2022**, *3*, 735–747.
136. Ruan, H.; Pan, N.; Wang, C.; et al. Functional UiO-66 series membranes with high perm selectivity of monovalent and bivalent anions for electrodialysis applications. *Ind. Eng. Chem. Res.* **2021**, *60*, 4086–4096.
137. Xu, T.; Shehzad, M.A.; Yu, D.; et al. Highly cation permselective metal-organic framework membranes with leaf-like morphology. *ChemSusChem* **2019**, *12*, 2593–2597.

138. Xu, T.; Shehzad, M.A.; Wang, X.; et al. Engineering leaf-like UiO-66-SO_3H membranes for selective transport of cations. *Nano-Micro Lett.* **2020**, *12*, 1–11.
139. Fan, J.; Wu, W.; Lu, Z.; et al. Rapid synthesis strategy of ultrathin UiO-66 separation membranes: Ultrasonic-assisted nucleation followed with microwave-assisted growth. *J. Membr. Sci.* **2022**, *664*, 121085.
140. Zhang, Y.; Sun, S.; Wang, M.; et al. Rationally engineered metal-organic framework membrane structure for effective Mg^{2+}/Li^{+} separation. *Chem. Eng. J.* **2025**, *525*, 170104.
141. Zhang, C.; Mu, Y.; Zhang, W.; et al. PVC-based hybrid membranes containing metal-organic frameworks for Li^{+}/Mg^{2+} separation. *J. Membr. Sci.* **2020**, *596*, 117724.
142. Zhao, C.; Feng, F.; Hou, J.; et al. Unlocking direct lithium extraction in harsh conditions through thiol-functionalized metal-organic framework subnanofluidic membranes. *J. Am. Chem. Soc.* **2024**, *146*, 14058–14066.